

AD-A274 713



2

PL-TR-93-2193

ELASTIC SCATTERING BY A SPHERICAL INCLUSION

Valeri A. Korneev and Lane R. Johnson

**Seismographic Station
University of California
Berkeley, CA 94720**

30 August 1993

DTIC
ELECTE
JAN 19 1994
S E D

**Final Report
12 September 1990-31 August 1993**

94-01679

54p

APPROVED FOR PUBLIC RELEASE; DISTRIBUTION UNLIMITED




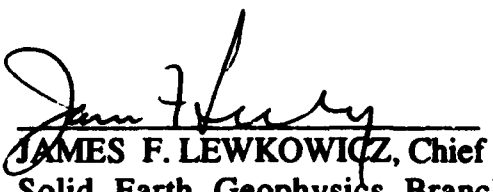
**PHILLIPS LABORATORY
Directorate of Geophysics
AIR FORCE MATERIEL COMMAND
HANSCOM AFB, MA 01731-3010**

94 1 14 069

The views and conclusions contained in this document are those of the authors and should not be interpreted as representing the official policies, either expressed or implied, of the Air Force or the U.S. Government.

This technical report has been reviewed and is approved for publication.


JAMES F. LEWKOWICZ
Program Manager


JAMES F. LEWKOWICZ, Chief
Solid Earth Geophysics Branch


DONALD H. ECKHARDT, Director
Earth Sciences Division

Qualified requestors may obtain additional copies from the Defense Technical Information Center.

If your address has changed, or if you wish to be removed from the mailing list, or if the addressee is no longer employed by your organization, please notify PL/TSI, 29 Randolph Road, Hanscom AFB MA 01731-3010. This will assist us in maintaining a current mailing list.

Do not return copies of this report unless contractual obligations or notices on a specific document require that it be returned.

REPORT DOCUMENTATION PAGE			Form Approved OMB No. 0704-0188	
<small>Public reporting burden for this collection of information is estimated to average 1 hour per response, including the time for reviewing instructions, searching existing data sources, gathering and maintaining the data needed, and completing and reviewing the collection of information. Send comments regarding this burden estimate or any other aspect of this collection of information, including suggestions for reducing this burden, to Washington Headquarters Services, Directorate for Information Operations and Reports, 1215 Jefferson Davis Highway, Suite 1204, Arlington, VA 22202-4302, and to the Office of Management and Budget, Paperwork Reduction Project (0704-0188), Washington, DC 20503.</small>				
1. AGENCY USE ONLY (Leave blank)		2. REPORT DATE 30 August 1993		3. REPORT TYPE AND DATES COVERED Final Report 12 Sep 1990 - 31 Aug 1993
4. TITLE AND SUBTITLE Elastic Scattering by a Spherical Inclusion			5. FUNDING NUMBERS PE 62101F PR 7600 TA 09 WU BF Contract F19628-90-K-0055	
6. AUTHOR(S) Valeri A. Korneev Lane R. Johnson				
7. PERFORMING ORGANIZATION NAME(S) AND ADDRESS(ES) University of California Seismographic Station Berkeley, CA 94720			8. PERFORMING ORGANIZATION REPORT NUMBER	
9. SPONSORING/MONITORING AGENCY NAME(S) AND ADDRESS(ES) Phillips Laboratory 29 Randolph Road Hanscom AFB, MA 01731-3010 Contract Manager: James Lewkowicz/GPEH			10. SPONSORING/MONITORING AGENCY REPORT NUMBER PL-TR-93-2193	
11. SUPPLEMENTARY NOTES				
12a. DISTRIBUTION / AVAILABILITY STATEMENT Approved for public release; Distribution unlimited			12b. DISTRIBUTION CODE	
13. ABSTRACT (Maximum 200 words) <p>The scattering problem of an arbitrary elastic wave incident upon a spherically symmetric inclusion is considered. General results expressed in the form of canonical scattering coefficients are obtained for the cases of incident P waves and incident S waves. Optical theorems relating the scattering cross-section to the amplitude of the scattered field in the forward direction are also derived for both of these cases. Analytical expressions for scattering coefficients of a homogeneous elastic sphere, a sphere filled by fluid, and a spherical cavity are presented, and scattering cross-sections are calculated for these different types of obstacles. It is shown that the scattering scale factor for low frequencies is defined by the wavelength of the scattered wave rather than the wavelength of the incident wave. A general finding is that the intensity of the $P \rightarrow S$ scattering is much stronger than the $S \rightarrow P$ scattering. For high-contrast inclusions the $P \rightarrow S$ scattering remains large for all frequencies and can be greater than the $P \rightarrow P$ scattering at low frequencies. Low velocity fluid inclusions have a resonant type of scattering with numerous peaks in the spectrum.</p> <p>Various approximate solutions are derived from the exact solutions, including the low contrast (Born) case and the low frequency (Rayleigh) case. The modifications of the low contrast solution necessary to maintain conservation of energy are discussed. Low-frequency asymptotics of the scattering coefficients for a homogeneous sphere of arbitrary contrast are obtained together with expressions for the scattered fields from both P and S incident waves. These expressions can be used for energy absorbing inclusions by assigning complex values to the elastic parameters. Waves scattered by the earth's core are examined as an example of high-frequency scattering.</p>				
14. SUBJECT TERMS elastic waves, sphere, scattering, diffraction			15. NUMBER OF PAGES 54	
			16. PRICE CODE	
17. SECURITY CLASSIFICATION OF REPORT Unclassified	18. SECURITY CLASSIFICATION OF THIS PAGE Unclassified	19. SECURITY CLASSIFICATION OF ABSTRACT Unclassified	20. LIMITATION OF ABSTRACT SAR	

Elastic scattering by a spherical inclusion*Valeri A. Korneev and Lane R. Johnson*

Center for Computational Seismology, Lawrence Berkeley Laboratory,
and Seismographic Station, University of California,
Berkeley, California 94720

Accession For	
NTIS	CRA&I
DTIC	TAB
Unannounced	
Justification	
By	
Distribution /	
Availability Codes	
Dist	Avail and/or Special
A-1	

1. Introduction

The earth is inhomogeneous on a wide range of scales and a variety of methods have been developed in seismology for analyzing the effects of these inhomogeneities. The theory of wave scattering, as developed in the fields of optics and acoustics, has been adapted to the case of elastic waves and has been quite useful in studying certain types of these inhomogeneities. For instance, Aki (1973) used scattering theory to study the phase and amplitude fluctuations of waves arriving at a seismic array, Haddon and Cleary (1974) interpreted the precursors to PKIKP as due to scattering near the mantle-core boundary, Aki (1969) attributed the coda waves from local earthquakes to scattering in the lithosphere, and Aki (1980) considered the role of scattering in the attenuation of waves. In parallel with these applications of scattering, the necessary extensions in the theory of elastic wave scattering were also developed. Korneev and Johnson (1993a, 1993b) discuss the background for both the exact and approximate theoretical developments in this area. Of particular interest to the subject of this paper are the excellent studies by Wu and Aki (1985a, 1985b).

The full treatment of elastic wave scattering is not a simple task, and most seismological studies have employed various approximations in their use of scattering theory. These include the assumption of only one type of wave (acoustic approximation), the assumption of a low contrast in material properties (Born approximation), and the assumption of low frequencies (Rayleigh approximation). While these approximations appear to be reasonable in many cases, a rigorous justification of their use is difficult. One method of checking the validity of the approximations is to compare them with exact analytical solutions. The purpose of this paper is to develop and discuss the properties of one such solution, the scattering of plane P waves and S waves by a spherical inclusion.

A spherical inclusion is the most convenient choice as a test model for comparison with approximate solutions. It is one of the few objects for which the scattering problem has an exact and computationally tractable solution, and it has the desirable property of being describable by a minimum number

of parameters. The treatment of the canonical scattering problem for the sphere has a long history. For light scattering it was formulated by Mie (1908) in terms of a series of spherical harmonics, and a comprehensive discussion of this topic can be found in Van der Hulst (1957). Elastic scattering by spherical obstacles has also been the subject of many publications, with some authors using potentials in their approach to the problem (Ying and Truell, 1956; Truell et. al., 1969; Yamakawa, 1962; Nigul et. al., 1974; Morozhnik, 1983a, 1983b) and others using displacements (Petrashen, 1946, 1950a, 1950b, 1953; Korneev and Petrashen, 1987). The present paper follows this latter approach and a detailed treatment of the analytical and numerical aspects of the scattering problem for P waves incident upon a spherical inclusion can be found in Korneev and Johnson (1993a), with a discussion of various approximate solutions in Korneev and Johnson (1993b). These results are extended in the present paper to the case of an incident S wave so that comparisons can be made between the relative scattering of P waves and S waves by various types of spherical inclusions.

2. Statement of the problem

Consider a two-part isotropic medium consisting of a spherically symmetric inclusion V_1 (part $v = 1$) with radius $r = R$ having elastic parameters $\lambda_1 = \lambda_1(r)$, $\mu_1 = \mu_1(r)$ and density $\rho_1 = \rho_1(r)$ which is embedded in a homogeneous elastic surrounding medium (part $v = 2$) having elastic parameters $\lambda = \lambda_2$, $\mu = \mu_2$ and density $\rho = \rho_2$. The inclusion V_1 may contain a number of internal shells which are bounded by spherical interfaces where the material properties or their spatial derivatives are radially discontinuous. The boundary conditions on such interfaces as well as those at the surface $r = R$ are linear and homogeneous. We assume that all elastic displacement fields under consideration have harmonic time dependence of the form $e^{i\omega t}$ where ω is the angular frequency. Joint Cartesian $\{x,y,z\}$ and spherical $\{r,\theta,\phi\}$ coordinate systems with the origin at the center of the inclusion will be used.

Incident from medium $v = 2$ is a harmonic disturbance with a displacement field given by

$$\tilde{U}_0 = U_0(x,y,z) e^{i\omega t} \quad (2.1)$$

The interaction of this incident wave with the inclusion gives rise to additional displacement fields both inside and outside the inclusion, and these are denoted by

$$U_v = U_v(x,y,z) , \quad (v = 1,2) \quad (2.2)$$

Since we will be primarily interested in the properties of the additional disturbance outside the inclusion, this field with subscript 2 will be referred to as the scattered field $U_{sc} = U_2$. Thus, the total field

U in the outer medium $v = 2$ is a sum of the incident wave and scattered field

$$U = U_0 + U_{sc} \quad (2.3)$$

The field U , as well as both of its individual components, must satisfy the equation of motion for a homogeneous isotropic elastic medium.

$$(\lambda + 2\mu) \nabla^2 U - \mu \nabla \times \nabla \times U + \rho \omega^2 U = 0 \quad (2.4)$$

The equation of motion in any spherical shell within the inclusion has the form

$$\begin{aligned} (\lambda_1 + 2\mu_1) \nabla^2 U_1 - \mu_1 \nabla \times \nabla \times U_1 + \frac{\partial \lambda_1}{\partial r} \nabla \cdot U_1 \hat{r} \\ + 2 \frac{\partial \mu_1}{\partial r} \frac{\partial U_1}{\partial r} + \frac{\partial \mu_1}{\partial r} [\hat{r} \times \nabla \times U_1] + \rho_1 \omega^2 U_1 = 0 \end{aligned} \quad (2.5)$$

We denote the velocities of the compressional and shear waves by

$$V_p^{(v)} = \sqrt{\frac{\lambda_v + 2\mu_v}{\rho_v}}, \quad V_s^{(v)} = \sqrt{\frac{\mu_v}{\rho_v}} \quad (2.6)$$

We require that the scattered field satisfy a radiation condition at large distances from the inclusion

$$U_{sc} = \frac{A_p(\theta, \phi)}{r} e^{-ik_p r} + \frac{A_s(\theta, \phi)}{r} e^{-ik_s r}, \quad (r \rightarrow \infty) \quad (2.7)$$

where $k_p = \omega/V_p^{(2)}$ and $k_s = \omega/V_s^{(2)}$. The functions $A_p(\theta, \phi)$ and $A_s(\theta, \phi)$ will be referred to as scattering diagrams of compressional and shear waves, respectively.

3. Spherical vectors

The solution will be developed using the spherical vector system of Petrashen (1945, 1949). A fairly complete description of this system can be found in Korneev and Johnson (1993a), so only the essential elements of the system will be listed here. The basis vectors for the system are

$$\begin{aligned} Y_{lm}^0 &= Y_{lm}^0(\theta, \phi) = r \times \nabla Y_{lm}(\theta, \phi) \\ Y_{lm}^+ &= Y_{lm}^+(\theta, \phi) = (l+1) \hat{r} Y_{lm}(\theta, \phi) - r \nabla Y_{lm}(\theta, \phi) \\ Y_{lm}^- &= Y_{lm}^-(\theta, \phi) = l \hat{r} Y_{lm}(\theta, \phi) + r \nabla Y_{lm}(\theta, \phi) \end{aligned} \quad (3.1)$$

with the usual definition of the spherical harmonic functions

$$Y_{lm}(\theta, \phi) = e^{im\phi} P_l^m(\cos \theta), \quad l \geq 0, \quad (-l \leq m \leq l)$$

The vectors of this system are linearly independent at any point (θ, ϕ) on a spherical surface. For $l = 0$

only the one vector $Y_{00}^+ = f$ is nonzero.

In the space of vector functions $f(\theta, \phi)$ defined on the spherical surface Ω

$$0 \leq \theta \leq \pi, \quad 0 \leq \phi \leq 2\pi, \quad d\Omega = \sin\theta \, d\theta \, d\phi$$

the basis vectors satisfy the orthogonality relation

$$\int_{\Omega} Y_{lm}^{*(\kappa)} \cdot Y_{l'm'}^{(\kappa)} \, d\Omega = [c_{lm}^{(\kappa)}]^{-2} \delta_{\kappa\kappa'} \delta_{ll'} \delta_{mm'} \quad (3.2)$$

where the normalizing coefficients are given by the expressions

$$\begin{aligned} c_{lm}^0 &= \sqrt{\frac{2l+1}{4\pi l(l+1)} \cdot \frac{(l-m)!}{(l+m)!}} \\ c_{lm}^+ &= \sqrt{\frac{1}{4\pi(l+1)} \cdot \frac{(l-m)!}{(l+m)!}} \\ c_{lm}^- &= \sqrt{\frac{1}{4\pi l} \cdot \frac{(l-m)!}{(l+m)!}} \end{aligned} \quad (3.3)$$

For vector functions $f(\theta, \phi)$ with a finite norm

$$\int_{\Omega} |f|^2 \, d\Omega = \int_{\Omega} f^* \cdot f \, d\Omega < \infty$$

the system of spherical vectors (3.1) is complete in the sense of convergence in the mean for a generalized Fourier series expansion of $f(\theta, \phi)$

$$f(\theta, \phi) = \sum_{\kappa=0, \pm 1} \sum_{l=0}^{\infty} \sum_{m=-l}^l a_{lm}^{(\kappa)} Y_{lm}^{(\kappa)}(\theta, \phi) \quad (3.4)$$

where

$$a_{lm}^{(\kappa)} = [c_{lm}^{(\kappa)}]^2 \int_{\Omega} Y_{lm}^{*(\kappa)} \cdot f \, d\Omega \quad (3.5)$$

Using the completeness of the vector system (3.1), we can seek a solution of our scattering problem in a form of a series

$$U(r, \theta, \phi) = \sum_{\kappa, l, m} d_{lm}^{(\kappa)} \psi_{lm}^{(\kappa)}(r) Y_{lm}^{(\kappa)}(\theta, \phi) \quad (3.6)$$

Because of the spherical symmetry of the present problem, the 3-D scattering problem is reduced to a 1-D boundary problem which must be solved for the radial functions $\psi_{lm}^{(\kappa)}(r)$. If the field U is known on any spherical surface $r = \text{constant}$, then the expansion coefficients of (3.6) can be determined using the orthogonality of the spherical vectors

$$d_{lm}^{(k)} \psi_{lm}^{(k)}(r) = \left[c_{lm}^{(k)} \right]^2 \int_{\Omega} Y_{lm}^{(k)}(\theta, \phi) \cdot U(r, \theta, \phi) d\Omega \quad (3.7)$$

4. Basic expressions

In the case of elastic wave propagation in a medium with spherical symmetry a critical element is the traction vector on a surface $r = \text{constant}$, which has the form

$$\mathbf{t}_r(\mathbf{U}) = \lambda \nabla \cdot \mathbf{U} \mathbf{f} + 2\mu \frac{\partial \mathbf{U}}{\partial r} + \mu [\mathbf{f} \times \nabla \times \mathbf{U}] \quad (4.1)$$

If the field \mathbf{U} is taken to have the form (3.6), then the corresponding traction vector has the form

$$\mathbf{t}_r(\mathbf{U}) = \sum_{k,l,m} T_{lm}^{(k)}(r) Y_{lm}^{(k)}(\theta, \phi) \quad (4.2)$$

where the expansion coefficients are given by

$$T_{lm}^0(r) = d_{lm}^0 \mu \left[\frac{\partial \psi_{lm}^0}{\partial r} - \frac{\psi_{lm}^0}{r} \right] \quad (4.3)$$

$$T_{00}^+(r) = d_{00}^+ \left[(\lambda + 2\mu) \left(\frac{\partial \psi_{00}^+}{\partial r} + 2 \frac{\psi_{00}^+}{r} \right) - 4\mu \frac{\psi_{00}^+}{r} \right] \quad (4.4a)$$

$$T_{lm}^+(r) = \frac{d_{lm}^+}{2l+1} \left[\left[(l+1)\lambda + (3l+2)\mu \right] \frac{\partial \psi_{lm}^+}{\partial r} + (l+2) \left[(l+1)\lambda - l\mu \right] \frac{\psi_{lm}^+}{r} \right] \\ + d_{lm}^- \frac{l(\lambda + \mu)}{2l+1} \left[\frac{\partial \psi_{lm}^-}{\partial r} - (l-1) \frac{\psi_{lm}^-}{r} \right] \quad (4.4b)$$

$$T_{lm}^-(r) = d_{lm}^- \frac{(l+1)(\lambda + \mu)}{2l+1} \left[\frac{\partial \psi_{lm}^+}{\partial r} + (l+2) \frac{\psi_{lm}^+}{r} \right] \\ + \frac{d_{lm}^-}{2l+1} \left[\left[l\lambda + (3l+1)\mu \right] \frac{\partial \psi_{lm}^-}{\partial r} + (l-1) \left[(l+1)\mu - l\lambda \right] \frac{\psi_{lm}^-}{r} \right] \quad (4.5)$$

Note that the coefficient $d_{lm}^{(0)}$ remains coupled with the same vector $Y_{lm}^{(0)}(\theta, \phi)$ in the expressions for both the displacement (3.6) and the traction (4.2). Differential equations for the radial functions $\psi_{lm}^{(k)}(r)$ can be obtained by substituting (3.6) into (2.5) and using the orthogonality of the spherical vectors. Solutions in the form of power series for the general case can be found in Korneev (1983), but in this paper the emphasis will be on the special case of a homogeneous sphere.

In the dynamic theory of elasticity it is useful to consider displacement field as a sum of potential (P) and solenoidal (S) fields

$$\mathbf{U} = \mathbf{U}_p + \mathbf{U}_s \quad (4.6)$$

which satisfy the conditions

$$\nabla \times \mathbf{U}_p = 0, \quad \nabla \cdot \mathbf{U}_s = 0 \quad (4.7)$$

and represent compressional and shear waves, respectively. Since $\nabla \cdot \psi(r) \mathbf{Y}_{lm}^0(\theta, \phi) = 0$ and $\nabla \times \psi(r) \mathbf{Y}_{00}^+ = 0$ the fields (4.6) have the form

$$\mathbf{U}_p = \sum_{l \geq 0, |m| \leq l} \left\{ F_{lm}^+(r) \mathbf{Y}_{lm}^+ + F_{lm}^-(r) \mathbf{Y}_{lm}^- \right\} \quad (4.8)$$

$$\mathbf{U}_s = \sum_{l \geq 1, |m| \leq l} \left\{ f_{lm}^0(r) \mathbf{Y}_{lm}^0 + f_{lm}^+(r) \mathbf{Y}_{lm}^+ + f_{lm}^-(r) \mathbf{Y}_{lm}^- \right\} \quad (4.9)$$

where for $l \geq 1$ the radial functions must satisfy the equations

$$\frac{\partial F_{lm}^-}{\partial r} - (l-1) \frac{F_{lm}^-}{r} - \frac{\partial F_{lm}^+}{\partial r} - (l+2) \frac{F_{lm}^+}{r} = 0, \quad (4.10)$$

$$l \left[\frac{\partial f_{lm}^-}{\partial r} - (l-1) \frac{f_{lm}^-}{r} \right] + (l+1) \left[\frac{\partial f_{lm}^+}{\partial r} + (l+2) \frac{f_{lm}^+}{r} \right] = 0, \quad (4.11)$$

In the case of a homogeneous isotropic elastic medium the displacement field \mathbf{U} must satisfy the equation of motion (2.4). Substituting the expressions (4.8) and (4.9) into (2.4) and using the orthogonality of the spherical vectors, one obtains differential equations of the second order for the radial functions. These equations have general solutions of the form

$$\begin{aligned} F_{lm}^+(r) &= a_{lm}^{1+} j_{l+1}(k_p r) + a_{lm}^{2+} h_{l+1}(k_p r) \\ F_{lm}^-(r) &= a_{lm}^{1-} j_{l-1}(k_p r) + a_{lm}^{2-} h_{l-1}(k_p r) \\ f_{lm}^+(r) &= b_{lm}^{1+} j_{l+1}(k_s r) + b_{lm}^{2+} h_{l+1}(k_s r) \\ f_{lm}^-(r) &= b_{lm}^{1-} j_{l-1}(k_s r) + b_{lm}^{2-} h_{l-1}(k_s r) \\ f_{lm}^0(r) &= c_{lm}^{10} j_l(k_s r) + c_{lm}^{20} h_l(k_s r) \end{aligned} \quad (4.12)$$

The solutions here have been constructed as a linear combination of two independent solutions, the spherical Bessel functions $j_n(kr)$ and the spherical Hankel functions of the second kind $h_n(kr)$. Fields which are regular at the origin will contain only the spherical Bessel functions, whereas secondary scattered fields which must satisfy the radiation conditions of the form (2.7) when $r \rightarrow \infty$ will contain only the Hankel functions. The differential equations (4.10) and (4.11) in this case reduce to

$$a_{lm}^{v+} = -a_{lm}^{v-}, \quad (l+1)b_{lm}^{v+} = lb_{lm}^{v-}, \quad (v = 1, 2) \quad (4.13)$$

We assume that the incident wave U_0 is regular at the origin so the radial functions of this wave will contain only the spherical Bessel functions. Thus the general case for the incident field U_0 is given by the expression

$$U_0 = \sum_{l,m} \left\{ c_{lm}^0 j_l(k_s r) Y_{lm}^0 + \left[a_{lm}^0 j_{l+1}(k_p r) + l b_{lm}^0 j_{l+1}(k_s r) \right] Y_{lm}^+ + \left[-a_{lm}^0 j_{l-1}(k_p r) + (l+1) b_{lm}^0 j_{l-1}(k_s r) \right] Y_{lm}^- \right\} \quad (4.14)$$

with arbitrary coefficients a_{lm}^0 for the P disturbance and coefficients b_{lm}^0 , c_{lm}^0 for the S disturbance. Introducing a set of "canonical" incident waves defined as

$$\begin{aligned} P_{lm} &= j_{l+1}(k_p r) Y_{lm}^+(\theta, \phi) - j_{l-1}(k_p r) Y_{lm}^-(\theta, \phi) \\ SV_{lm} &= l j_{l+1}(k_s r) Y_{lm}^+(\theta, \phi) + (l+1) j_{l-1}(k_s r) Y_{lm}^-(\theta, \phi) \\ SH_{lm} &= j_l(k_s r) Y_{lm}^0(\theta, \phi) \end{aligned} \quad (4.15)$$

we can represent (4.14) as the linear combination

$$U_0 = \sum_{l,m} \left\{ a_{lm}^0 P_{lm} + b_{lm}^0 SV_{lm} + c_{lm}^0 SH_{lm} \right\} \quad (4.16)$$

Each of the waves of (4.15) satisfies the equation of motion (2.4). The wave P_{lm} is a pure compressional wave and SV_{lm} and SH_{lm} waves are both shear waves.

Now consider the incidence of canonical waves of the form (4.16) on the inclusion V_1 . Substitution of the field U_1 having the form (3.6) into the equation of motion (2.5) leads to a separate set of differential equations for radial functions for any pair of indices l, m . Moreover, the equation for determining $\psi_{lm}^0(r)$ separates from those for $\psi_{lm}^+(r)$ and $\psi_{lm}^-(r)$. Also note that azimuth index m is not present in any of the coefficients of the differential equations. The boundary conditions on the surface $r = R$ of the inclusion are required to be linear and homogeneous. For a welded elastic-elastic interface they have the form

$$U_1 = U_0 + U_{sc} \quad \text{and} \quad t_r^{(1)}[U_1] = t_r^{(2)}[U_0 + U_{sc}] \quad (4.17)$$

with the usual modifications for elastic-fluid and elastic-free interfaces. Again, because of the orthogonality of vectors (3.1), separate boundary equations may be obtained for any pair of indices l, m , and in the present problem these equations do not depend upon the index m . The canonical field P_{lm} will

excite in the medium $v = 2$ a scattered field of the form

$$U_{lm}^P = \left[a_l^{PP} h_{l+1}(k_p r) + l b_l^{PS} h_{l+1}(k_s r) \right] Y_{lm}^+ + \left[-a_l^{PP} h_{l-1}(k_p r) + (l+1) b_l^{PS} h_{l-1}(k_s r) \right] Y_{lm}^- \quad (4.18)$$

The canonical field SV_{lm} will excite in the medium $v = 2$ a scattered field

$$U_{lm}^{SV} = \left[a_l^{SP} h_{l+1}(k_p r) + l b_l^{SS} h_{l+1}(k_s r) \right] Y_{lm}^+ + \left[-a_l^{SP} h_{l-1}(k_p r) + (l+1) b_l^{SS} h_{l-1}(k_s r) \right] Y_{lm}^- \quad (4.19)$$

and the field SH_{lm} will excite in the medium $v = 2$ the scattered field

$$U_{lm}^{SH} = c_l^S h_l(k_s r) Y_{lm}^0 \quad (4.20)$$

The set of coefficients a_l^{PP} , a_l^{SP} , b_l^{SS} , b_l^{PS} , c_l^S which are contained in these expressions will be called the *canonical* scattering coefficients for the inclusion V_1 . They may be found as solutions of linear systems following substitution of the relevant expressions into the boundary conditions and using the orthogonality of the spherical vectors. Analytical formulas for these canonical scattering coefficients for the case of a homogeneous elastic spherical inclusion, as well as for the special cases of a fluid filled spherical inclusion and a spherical cavity, are given in Appendix A. These will be discussed in more detail later.

Once the canonical scattering coefficients are known, an incident field (4.16) specified by the coefficients a_{lm}^0 , b_{lm}^0 , c_{lm}^0 will generate a scattered field which can be written as

$$U_{sc} = \sum_{l,m} \left\{ c_{lm}^0 c_l^S h_l(k_s r) Y_{lm}^0 + \left[\left(a_{lm}^0 a_l^{PP} + b_{lm}^0 a_l^{SP} \right) h_{l+1}(k_p r) + l \left(a_{lm}^0 b_l^{PS} + b_{lm}^0 b_l^{SS} \right) h_{l+1}(k_s r) \right] Y_{lm}^+ + \left[- \left(a_{lm}^0 a_{l-1}^{PP} + b_{lm}^0 a_{l-1}^{SP} \right) h_{l-1}(k_p r) + (l+1) \left(a_{lm}^0 b_{l-1}^{PS} + b_{lm}^0 b_{l-1}^{SS} \right) h_{l-1}(k_s r) \right] Y_{lm}^- \right\} \quad (4.21)$$

This represents the complete solution for the scattered field from a spherical inclusion for an arbitrary incident wave.

The field U_1 inside of the sphere will have the general form of (3.6) and will be linearly dependent upon the source coefficients a_{lm}^0 , b_{lm}^0 , c_{lm}^0 . For the special case of a homogeneous isotropic material inside the inclusion, U_1 has the same form as (4.21) with all of the functions h_k replaced by the corresponding functions j_k and with a new set of canonical coefficients for the inner medium $v = 1$ ($r < R$). For the sake of completeness, analytical expressions for this internal set of canonical coefficients for the cases of elastic and fluid spheres can be found in Appendix B. However, throughout

the remainder of this paper only the scattered field outside of the inclusion will be considered.

One method of determining the coefficients a_{lm}^0 , b_{lm}^0 , and c_{lm}^0 of the incident wave is to use (3.7) and integrate the product of the incident field U_0 with the corresponding spherical vector. Thus, for the case of a plane P wave propagating in the direction of the positive z axis

$$U_0 = e^{-ik_p z} \hat{z} \quad (4.22)$$

and

$$a_{lm}^0 = e^{-i\frac{\pi}{2}(l+1)} \delta_{m,0} , \quad b_{lm}^0 = 0 , \quad c_{lm}^0 = 0 \quad (4.23)$$

For an incident plane S waves propagating in the direction of the positive z axis and polarized along the x axis

$$U_0 = e^{-ik_p z} \hat{x} \quad (4.24)$$

and

$$\begin{aligned} a_{lm}^0 &= 0 , \quad b_{lm}^0 = \frac{1}{2l(l+1)} \left[l(l+1)\delta_{m,-1} - \delta_{m,1} \right] e^{-i\frac{\pi}{2}(l+1)} \\ c_{lm}^0 &= -\frac{2l+1}{2l(l+1)} \left[l(l+1)\delta_{m,-1} + \delta_{m,1} \right] e^{-i\frac{\pi}{2}(l+1)} \end{aligned} \quad (4.25)$$

For a point pressure source located at the point $R_0 = (z_0, 0, 0)$ where $z_0 > R$

$$U_0 = -\nabla \frac{e^{-ik_p |r-R_0|}}{|r-R_0|} \quad (4.26)$$

and

$$a_{lm}^0 = -ik_p^2 h_l(k_p z_0) \delta_{m,0} , \quad b_{lm}^0 = 0 , \quad c_{lm}^0 = 0 \quad (4.27)$$

The scattered field (4.21), expressed in terms of spherical unit vectors $(\hat{r}, \hat{\theta}, \hat{\phi})$, for the cases of the incident plane P wave (4.22) and the incident plane S wave (4.24) are given in Appendix C.

The convergence of the series (4.21) depends upon the observation distance r , the canonical scattering coefficients, and the coefficients of the incident field, and each combination of these variables may require a special investigation. The basic problem is to estimate the number of terms that should be included in the series in order to achieve a certain level of accuracy. One general guideline is that the number of terms which are necessary in order to represent the incident wave on the surface of the inclusion at the desired accuracy is a good estimate of the number of terms required in the solution series. Korneev and Johnson (1993a) considered this problem for the scattering of a plane P wave and

showed that the necessary number of terms in the series could be estimated by the formula

$$l_0 = \frac{ek_p R}{2} + N \quad (4.28)$$

where R is the radius of the sphere and N is a constant. A value of $N = 15$ is sufficient to give an accuracy of 10^{-4} .

5. Flow of the scattered energy

A useful method of characterizing the scattering by an object is to calculate the energy of the scattered waves and compare it to the energy of the incident wave. Various forms of this ratio between the scattered and incident energies are called scattering cross sections. The energy of the scattered waves can be obtained by calculating the energy flux of scattered waves through a surface S that completely surrounds the object. Noting that the energy flux through a surface element ds having a normal n is given by $(\dot{U} \cdot t_n[U])$ and that the energy flux averaged over one period is $\omega \text{Im}\{U \cdot t_n^*[U]\}/2$, then the total energy flux per period through the surface S is given by

$$F = \frac{\omega}{2} \text{Im} \int_S (U \cdot t_n^*[U]) ds \quad (5.1)$$

where $(*)$ denotes the complex conjugate.

Substituting the total field (2.3) into (5.1) and assuming conservation of energy (no energy absorption by the material), we obtain

$$F = F_{sc} + 2F_c = \frac{\omega}{2} \text{Im} \int_S (U_{sc} \cdot t_n^*[U_{sc}]) ds + \omega \text{Im} \int_S (U_{sc} \cdot t_n^*[U_0]) ds = 0 \quad (5.2)$$

where F_{sc} is the total energy flow of the scattered field and F_c describes the energy of coherent interaction between the scattered field U_{sc} and the incident field U_0 . Physically, the phenomena of scattering describes the conversion of part of the energy of the primary incident wave into the energy of the secondary scattered waves. Therefore, after the incident wave has interacted with the inclusion, it should have lost part of its energy. However, the formal solution (2.3) leaves the incident wave undisturbed. This means that the additional field U_{sc} of (2.3) must include both the change in the primary wave along with the secondary scattered waves. We will return to this problem later when considering the scattering cross-sections of elastic spheres.

To calculate the energy flow F_{sc} of the scattered field (4.21) caused by the incident field (4.16) we need expressions for the tractions associated with both of these fields. Since total energy flow does

not depend from the shape of the surface S , we let S be a spherical surface of radius r , which is arbitrary so long as the inclusion is contained inside S . The traction vector $\mathbf{t}_r(\mathbf{U}_s)$ of the field \mathbf{U}_s on this surface has the form

$$\begin{aligned} \mathbf{t}_r(\mathbf{U}_s) = \sum_{l,m} \left\{ c_{lm}^0 c_l^s C_l \mathbf{Y}_{lm}^0 + \left[\left(a_{lm}^0 a_l^{PP} + b_{lm}^0 a_l^{SP} \right) A_l^+ + l \left(a_{lm}^0 b_l^{PS} + b_{lm}^0 b_l^{SS} \right) B_l^+ \right] \mathbf{Y}_{lm}^+ \right. \\ \left. + \left[\left(a_{lm}^0 a_l^{PP} + b_{lm}^0 a_l^{SP} \right) A_l^- - (l+1) \left(a_{lm}^0 b_l^{PS} + b_{lm}^0 b_l^{SS} \right) B_l^- \right] \mathbf{Y}_{lm}^- \right\} \end{aligned} \quad (5.3)$$

where

$$C_l = \frac{\mu}{r} \left[k_s r h_{l-1}(k_s r) - (l+2) h_l(k_s r) \right] \quad (5.4)$$

$$\left. \begin{aligned} A_l^+ \\ A_l^- \end{aligned} \right\} = \frac{\mu}{r} \left[\frac{k_p r}{\gamma^2} h_l(k_p r) - 2 \left\{ \begin{aligned} (l+2) h_{l+1}(k_p r) \\ (l-1) h_{l-1}(k_p r) \end{aligned} \right\} \right] \quad (5.5)$$

$$\left. \begin{aligned} B_l^+ \\ B_l^- \end{aligned} \right\} = \frac{\mu}{r} \left[k_s r h_l(k_s r) - 2 \left\{ \begin{aligned} (l+2) h_{l+1}(k_s r) \\ (l-1) h_{l-1}(k_s r) \end{aligned} \right\} \right] \quad (5.6)$$

The traction vector for the incidence field (4.16) can be obtained from (5.3) by setting all canonical scattering coefficients equal to one and by substituting for all spherical Hankel functions the corresponding Bessel function in (5.4)-(5.6).

After making all of the necessary substitutions in (5.2), performing the integration over S , and some tedious manipulations, we obtain

$$\begin{aligned} F_{sc} &= F_{sc}^P + F_{sc}^S \\ &= 2\pi(\lambda + 2\mu)V_p \sum_{l,m} (2l+1) \frac{(l+m)!}{(l-m)!} \left| a_{lm}^0 a_l^{PP} + b_{lm}^0 a_l^{SP} \right|^2 \\ &\quad + 2\pi(\lambda + 2\mu)V_p \sum_{l,m} (2l+1) \frac{(l+m)!}{(l-m)!} l(l+1) \gamma^3 \left[\frac{|c_{lm}^0 c_l^s|^2}{(2l+1)^2} + \left| a_{lm}^0 b_l^{PS} + b_{lm}^0 b_l^{SS} \right|^2 \right] \end{aligned} \quad (5.7a)$$

which can also be expressed as

$$\begin{aligned} F_{sc} &= -2\pi(\lambda + 2\mu)V_p \sum_{l,m} (2l+1) \frac{(l+m)!}{(l-m)!} \left\{ |a_{lm}^0|^2 \text{Re}\{a_l^{PP}\} + \text{Re}\{a_{lm}^{*0} b_{lm}^0 a_l^{SP}\} \right. \\ &\quad \left. + l(l+1) \gamma^3 \left[\frac{|c_{lm}^0|^2}{(2l+1)^2} \text{Re}\{c_l^s\} + |b_{lm}^0|^2 \text{Re}\{b_l^{SS}\} + \text{Re}\{a_{lm}^0 b_{lm}^{*0} b_l^{PS}\} \right] \right\} \end{aligned} \quad (5.7b)$$

This is an exact result. The part F_{sc}^P corresponds to the energy flow of the scattered P waves and the

part F'_x corresponds to the energy flow of the scattered S waves. As can be seen, the combined incidence of both P and S waves on the inclusion can cause constructive or destructive interference in the scattered field.

The equation (5.7) must be true for any set of coefficients for the incident wave (4.16), which leads to the following four independent relations between the canonical scattering coefficients

$$|c_l^S|^2 = -\text{Re}\{c_l^S\} \quad (5.8)$$

$$|a_l^{PP}|^2 + l(l+1)\gamma^3 |b_l^{PS}|^2 = -\text{Re}\{a_l^{PP}\} \quad (5.9)$$

$$|a_l^{SP}|^2 + l(l+1)\gamma^3 |b_l^{SS}|^2 = -l(l+1)\gamma^3 \text{Re}\{b_l^{SS}\} \quad (5.10)$$

$$2\left[a_l^{PP}a_l^{*SP} + l(l+1)\gamma^3 b_l^{PS}b_l^{*SS}\right] = -a_l^{*SP} - l(l+1)\gamma^3 b_l^{PS} \quad (5.11)$$

Multiplying (5.11) first by a_l^{SP} and then by b_l^{*PS} and eliminating the quantity $a_l^{SP}b_l^{PS}$ leads to the expression

$$\left|a_l^{SP}\right|^2 \left|1 + 2a_l^{PP}\right|^2 = l^2(l+1)^2\gamma^6 \left|b_l^{PS}\right|^2 \left|1 + 2b_l^{SS}\right|^2$$

Using the equivalences (5.9) and (5.10), this equation reduces to

$$\left|a_l^{SP}\right|^2 = l^2(l+1)^2\gamma^6 \left|b_l^{PS}\right|^2 \quad (5.12)$$

The equivalences (5.8)-(5.10) will be used in the next section in formulating optical theorems. The last equivalence (5.12) will be used later when considering the relation between $P \rightarrow S$ and $S \rightarrow P$ scattering. The equivalences (5.8)-(5.12) are also useful in verifying the accuracy of numerical calculations.

It is worth noting that the result (5.7) would also have been obtained if the radial functions had been reduced to their far field asymptotic expressions before substituting into (5.2). This means that the net energy flux due to the near-field terms in the solution is zero. However, as shown by Korneev and Johnson (1993a), these near-field terms can significantly affect the displacement field formed in the vicinity of the inclusion.

6. Scattering cross-sections and optical theorems

Here we consider the special cases of an incident field consisting of either a plane P wave or a plane S wave. Earlier we obtained the coefficients (4.23) and (4.25) which represent these waves in terms of the spherical vectors (3.1). Now we introduce the scattering cross-section σ as the ratio

$$\sigma = \frac{F_{sc}}{F_0} \quad (6.1)$$

which is the energy flow F_{sc} of the scattered field normalized by the energy flow F_0 of the incident wave per unit area normal to the direction of propagation.

We begin with the case of the incident plane P wave (4.23). For this wave the energy flow per unit area of the incident wave is

$$F_0^P = (\lambda + 2\mu)k_p \frac{\omega}{2} \quad (6.2)$$

Substituting coefficients (4.23) into (5.7) we get the scattering cross-section

$$\begin{aligned} \sigma^P &= \frac{F_{sc}^P}{F_0^P} = \sigma^{PP} + \sigma^{PS} \\ &= \frac{4\pi}{k_p^2} \sum_{l \geq 0} (2l + 1) \left\{ |a_l^{PP}|^2 + l(l+1) \gamma^3 |b_l^{PS}|^2 \right\} \end{aligned} \quad (6.3a)$$

$$= -\frac{4\pi}{k_p^2} \sum_{l \geq 0} (2l + 1) \operatorname{Re}\{a_l^{PP}\} \quad (6.3b)$$

On the other hand, putting the coefficients (4.23) into the expression (4.21) for the scattered field and using the asymptotic representation

$$h_l(z) \approx \frac{1}{z} e^{-i(z - \frac{\pi}{2}(l+1))}, \quad (z \gg l)$$

for the spherical Hankel functions, we obtain for $\theta = 0$

$$U_{sc}^P(0) = A_P(0) \frac{e^{-ik_p r}}{r} \hat{z} \quad (6.4)$$

where

$$A_P(0) = \frac{i}{k_p} \sum_{l \geq 0} (2l + 1) a_l^{PP} \quad (6.5)$$

Comparing (6.3) and (6.5) we have the equation

$$\sigma^P = -\frac{4\pi}{k_p} \operatorname{Im}\{A_P(0)\} \quad (6.6)$$

which is the optical theorem for an incident plane P wave. This equation establishes a connection between the scattering cross-section and the amplitude of the scattered field in the forward direction.

For an incident plane S wave (4.25) the procedure for obtaining an optical theorem is similar. The energy flow per unit area of the incident S wave is

$$F_0^S = \mu k_s \frac{\omega}{2} \quad (6.7)$$

Then, using the coefficients (4.25) in (5.7) we have

$$\begin{aligned} \sigma^S &= \frac{F_{sc}^S}{F_0^S} = \sigma^{SP} + \sigma^{SS} \\ &= \frac{2\pi}{\gamma^3 k_s^2} \sum_{l \geq 1} \frac{(2l+1)}{l(l+1)} |a_l^{SP}|^2 + \frac{2\pi}{k_s^2} \sum_{l \geq 1} (2l+1) \left[|b_l^{SS}|^2 + |c_l^S|^2 \right] \end{aligned} \quad (6.8a)$$

$$= -\frac{2\pi}{k_s^2} \sum_{l \geq 1} (2l+1) \operatorname{Re}\{b_l^{SS} + c_l^S\} \quad (6.8b)$$

The forward scattered shear wave in the far field has a form

$$U_{sc}^S(0) = A_S(0) \frac{e^{-ik_s r}}{r} \hat{x} \quad (6.9)$$

where

$$A_S(0) = \frac{i}{2k_s} \sum_{l \geq 1} (2l+1) \left[b_l^{SS} + c_l^S \right] \quad (6.10)$$

Comparing (6.8) and (6.10) we have

$$\sigma^S = -\frac{4\pi}{k_s} \operatorname{Im}\{A_S(0)\} \quad (6.11)$$

which is the optical theorem for an incident plane S wave. Optical theorems such as this and (6.6) can be useful in studying the attenuation of waves due to scattering.

7. Comparison of $P \rightarrow S$ and $S \rightarrow P$ scattering

The equivalence (5.12) allows one to compare scattering of converted waves for the same scatterer. Applying (5.12) to (6.3a) and (6.8a) we see that the scattering cross-sections for converted waves are connected by the simple relation

$$\sigma^{PS} = \frac{2}{\gamma^2} \sigma^{SP} \quad (7.1)$$

This equation says that the scattering cross-section of $P \rightarrow S$ converted waves is significantly larger than that for $S \rightarrow P$ converted waves. This result is valid for any spherically symmetric scatterer.

In practice one deals with the amplitudes of scattered waves, and so it is useful to also estimate the mean intensity (squared amplitude) of the field. Using the far field approximation, the mean intensity of the scattered field for an incident plane P wave has the form

$$\begin{aligned}
 I_P &= \frac{1}{4\pi} \int_{\Omega} |U_s|^2 d\Omega \\
 &= \frac{1}{k_p^2 r^2} \sum_{l \geq 0} (2l+1) \left\{ |a_l^{PP}|^2 + l(l+1)\gamma^2 |b_l^{PS}|^2 \right\} \\
 &= \frac{\sigma^{PP}}{4\pi r^2} + \frac{\sigma^{PS}}{4\pi \gamma r^2} = I_{PP} + I_{PS}
 \end{aligned} \tag{7.2}$$

where the integration is taken over a spherical surface at the radius $r > R$ in the far field zone. Similarly, for an incident plane S wave we have

$$\begin{aligned}
 I_S &= \frac{1}{4\pi} \int_{\Omega} |U_s|^2 d\Omega \\
 &= \frac{1}{\gamma^2 k_s^2 r^2} \sum_{l \geq 1} \frac{(2l+1)}{l(l+1)} |a_l^{SP}|^2 + \frac{1}{k_s^2 r^2} \sum_{l \geq 1} (2l+1) \left(|b_l^{SS}|^2 + |c_l^S|^2 \right) \\
 &= \gamma \frac{\sigma^{SP}}{4\pi r^2} + \frac{\sigma^{SS}}{4\pi r^2} = I_{SP} + I_{SS}
 \end{aligned} \tag{7.3}$$

Using the equivalence (5.12), we have for the ratio of the mean conversion intensities

$$\frac{I_{PS}}{I_{SP}} = \frac{1}{\gamma^2} \frac{\sigma^{PS}}{\sigma^{SP}} = \frac{2}{\gamma^4} = 2 \frac{(\lambda + 2\mu)^2}{\mu^2} \tag{7.4}$$

Thus, if the comparison is made between the intensities of the waves rather than the energy flux of (7.1), the asymmetry in the average conversion between P and S waves by scattering is even larger. Note that this is a general result that holds for all frequencies. For the "typical" seismic situation where $\gamma = 1/\sqrt{3}$, the ratio (7.4) is equal to 18. For soft media, where γ is even smaller in a relative sense, this ratio could be significantly larger.

For the case of homogeneous spherical inclusion (elastic, fluid, or cavity), an even stronger result can be obtained which involves no spatial averaging. First note that the converted far field for the incident plane P wave (4.22) is easily obtained from (C.1) and has the form

$$U_{PS} = -i \sum_{l \geq 1} (2l+1) b_l^{PS} \frac{e^{-k_s r}}{k_s r} \frac{\partial P_l(\cos \theta)}{\partial \theta} \hat{\theta} = A_{PS}(\omega, \theta) \frac{e^{-k_s r}}{r} \hat{\theta} \tag{7.5}$$

where $A_{PS}(\omega, \theta)$ is a scattering coefficient for converted $P \rightarrow S$ waves. Similarly, for the incident plane S wave (4.24) the converted far field can be derived from (C.3)

$$U_{SP} = -i \cos\phi \sum_{l \geq 1} \frac{(2l+1)}{l(l+1)} a_l^{SP} \frac{e^{-i k_p r}}{k_p r} P_l^1(\cos\theta) \hat{r} = A_{SP}(\omega, \theta, \phi) \frac{e^{-i k_p r}}{r} \hat{r} \quad (7.6)$$

with the scattering coefficient $A_{SP}(\omega, \theta, \phi)$. Now for the case of a homogeneous inclusion it follows from the solutions listed in Appendix A that

$$a_l^{SP} = \gamma_2^3 l(l+1) b_l^{PS} \quad (7.7)$$

Using (7.7) in (7.5) and (7.6) we have the relation

$$A_{SP}(\omega, \theta, \phi) = -\gamma_2^2 \cos\phi A_{PS}(\omega, \theta) \quad (7.8)$$

Thus, in the far field the scattering coefficients of the converted waves have the same functional dependence on frequency ω and angle θ . For the case of an incident P wave the problem has axial symmetry so A_{PS} has no dependence upon ϕ , but this is not true of A_{SP} .

Aki (1992) arrives at a results similar to (7.4) and (7.8) using a more general approach involving the reciprocal theorem. He considered only the case where the polarization of the P and S waves was in the same plane ($\phi = 0$), and thus obtained an equation similar to (7.8) without the $\cos\phi$ term. Consequently, because the average value of $\cos^2\phi$ is 1/2, his equation for the squared amplitudes does not contain the factor of 2 found in (7.4). The approach of Aki (1992) is extended in Appendix D to consider polarized S waves and it is shown that general reciprocal relations can be established in the far field for an arbitrary localized scatterer. However, it appears that results such as (7.8), which involve total amplitudes of the P and S waves incident from the same direction, can only be established for scatterers with a high degree of symmetry.

8. Homogeneous sphere

The results that have been presented up to this point are valid for any inclusion that has spherical symmetry. To proceed further requires that solutions be obtained for the canonical scattering coefficients, and in order to do this it is necessary to specify the internal structure of the inclusion. Here we consider the special case where the material properties of the inclusion are independent of the radial coordinate, in which case it is possible to obtain analytical solutions for the canonical scattering coefficients.

The scattering of plane P waves by a homogeneous sphere was treated in our previous papers (Korneev and Johnson, 1992a, 1993b) where detailed interpretations of the scattered fields were

presented. That set of solutions has been expanded to include the scattering of S waves and the complete set of canonical scattering coefficients for a homogeneous spherical inclusion is given in Appendix A. In addition to the elastic inclusion, formulas are also given for the special cases of a fluid inclusion and an empty cavity.

Consider the solutions given in Appendix A in the limit of low frequency. Then the most significant scattering coefficients are given by the asymptotic expressions

$$a_0^{PP} = i \frac{\xi^3}{6} \frac{\frac{3}{2}(\lambda_1 - \lambda_2) + \mu_1 - \mu_2}{\frac{1}{2} \left(\frac{3}{2}\lambda_1 + \mu_1 \right) + \mu_2} \quad (8.1)$$

$$a_1^{PP} = -i \frac{\xi^3}{9} \left[\frac{\rho_1}{\rho_2} - 1 \right], \quad b_1^{PS} = i \frac{\eta^3}{9} \left[\frac{\rho_1}{\rho_2} - 1 \right] \quad (8.2)$$

$$a_2^{PP} = i \xi^3 \frac{4}{45} \left[\frac{\mu_1}{\mu_2} - 1 \right] \frac{\gamma^2}{D}, \quad b_2^{PS} = -i \eta^3 \frac{2}{45} \left[\frac{\mu_1}{\mu_2} - 1 \right] \frac{\gamma}{D} \quad (8.3)$$

$$a_1^{SP} = i \xi^3 \frac{2}{9} \left[\frac{\rho_1}{\rho_2} - 1 \right], \quad b_1^{SS} = -i \eta^3 \frac{2}{9} \left[\frac{\rho_1}{\rho_2} - 1 \right] \quad (8.4)$$

$$a_2^{SP} = -i \xi^3 \frac{4}{45} \left[\frac{\mu_1}{\mu_2} - 1 \right] \frac{\gamma}{D}, \quad b_2^{SS} = i \eta^3 \frac{2}{15} \left[\frac{\mu_1}{\mu_2} - 1 \right] \frac{1}{D} \quad (8.5)$$

$$c_1^S = -i \frac{\eta^5}{45} \left[\frac{\rho_1}{\rho_2} - 1 \right], \quad c_2^S = i \frac{\eta^5}{45} \frac{\mu_1 - \mu_2}{4\mu_2 + \mu_1} \quad (8.6)$$

where

$$\xi = k_p R, \quad \eta = k_s R \quad (8.7)$$

$$\gamma = \frac{V_s}{V_p}, \quad D = 1 + \frac{2}{15} \left[\frac{\mu_1}{\mu_2} - 1 \right] (3 + 2\gamma^2) \quad (8.8)$$

The coefficients c_1^S and c_2^S are obviously much smaller than the others and may be neglected at low frequencies. The case of a fluid inclusion is easily obtained from (8.1)-(8.5) by putting $\mu_1 = 0$. The coefficients (8.1)-(8.5) may also be considered for the case of intrinsic attenuation inside the inclusion by assuming that the elastic parameters λ_1 and μ_1 have complex values. In this case the coefficients for $l = 1$ depend only upon the density contrast of the inclusion, whereas the other coefficients in the limit of large intrinsic attenuation go to the values

$$a_0^{PP} = i \frac{\xi^3}{3}, \quad a_2^{PP} = i 2 \xi^3 \frac{\gamma^2}{3 + 2\gamma^2}, \quad b_2^{PS} = -i \frac{\eta^3}{3} \frac{\gamma}{3 + 2\gamma^2} \quad (8.9)$$

$$a_2^{SP} = -i2\xi^3 \frac{\gamma}{3+2\gamma^2}, \quad b_2^{SY} = i\eta^3 \frac{1}{3+2\gamma^2} \quad (8.10)$$

These formulas represent the case of a small absorbing inclusion which captures all of the energy which crosses its boundary.

It is convenient to describe the energy scattered by a homogeneous spherical inclusion with a non-dimensional normalized scattering cross section. Dividing the σ from (6.1) by the area of the geometrical shadow, we have

$$\sigma_N = \frac{\sigma}{\pi R^2} \quad (8.11)$$

For an incident P wave in the low-frequency limit we have

$$\begin{aligned} \sigma_N^P &= \sigma_N^{PP} + \sigma_N^{PS} = \frac{4}{9}\xi^4 \left\{ \left| \frac{\frac{3}{2}(\lambda_1 - \lambda_2) + \mu_1 - \mu_2}{\frac{3}{2}\lambda_1 + \mu_1 + 2\mu_2} \right|^2 + \frac{1}{3} \left(\frac{\rho_1}{\rho_2} - 1 \right)^2 + \frac{16}{45}\gamma^2 \left| \frac{\mu_1 - \mu_2}{\mu_2 D} \right|^2 \right\} \\ &\quad + \frac{8}{27}\xi^4 \left\{ \frac{1}{\gamma^2} \left(\frac{\rho_1}{\rho_2} - 1 \right)^2 + \frac{4}{5} \left| \frac{\mu_1 - \mu_2}{\mu_2 D} \right|^2 \right\} \\ &= \frac{4}{9}\xi^4 \left\{ \left| \frac{\frac{3}{2}(\lambda_1 - \lambda_2) + \mu_1 - \mu_2}{\frac{3}{2}\lambda_1 + \mu_1 + 2\mu_2} \right|^2 + \frac{1}{3} \left(\frac{\rho_1}{\rho_2} - 1 \right)^2 \left(1 + \frac{2}{\gamma^2} \right) + \frac{8}{45}\gamma^2 \left| \frac{\mu_1 - \mu_2}{\mu_2 D} \right|^2 \left(2\gamma^2 + \frac{3}{\gamma^2} \right) \right\} \quad (8.12) \end{aligned}$$

Similarly, for an incident S wave we get

$$\begin{aligned} \sigma_N^S &= \sigma_N^{SP} + \sigma_N^{SY} = \frac{4}{27}\eta^4 \gamma^3 \left\{ \left(\frac{\rho_1}{\rho_2} - 1 \right)^2 + \frac{4}{5}\gamma^2 \left| \frac{\mu_1 - \mu_2}{\mu_2 D} \right|^2 \right\} \\ &\quad + \frac{8}{27}\eta^4 \left\{ \left(\frac{\rho_1}{\rho_2} - 1 \right)^2 + \frac{3}{5} \left| \frac{\mu_1 - \mu_2}{\mu_2 D} \right|^2 \right\} \\ &= \frac{4}{27}\eta^4 \left\{ \left(\frac{\rho_1}{\rho_2} - 1 \right)^2 (\gamma^3 + 2) + \frac{2}{5}(2\gamma^5 + 3) \left| \frac{\mu_1 - \mu_2}{\mu_2 D} \right|^2 \right\} \quad (8.13) \end{aligned}$$

For the low-contrast case, where

$$\frac{|\delta\lambda|}{\lambda} = \frac{|\lambda_1 - \lambda_2|}{\lambda} \ll 1, \quad \frac{|\delta\mu|}{\mu} = \frac{|\mu_1 - \mu_2|}{\mu} \ll 1, \quad \frac{|\delta\rho|}{\rho} = \frac{|\rho_1 - \rho_2|}{\rho} \ll 1 \quad (8.14)$$

the expressions (8.12) and (8.13) can be simplified to

$$\sigma_N^P = \frac{4}{27}\xi^4 \left\{ \frac{1}{3} \left| \frac{3\delta\lambda + 2\delta\mu}{\lambda + 2\mu} \right|^2 + \left(\frac{\delta\rho}{\rho} \right)^2 \left(1 + \frac{2}{\gamma^2} \right) + \frac{8}{15} \left| \frac{\delta\mu}{\mu} \right|^2 \gamma^2 \left(2\gamma^2 + \frac{3}{\gamma^2} \right) \right\}$$

$$= \frac{4}{27} \eta \left\{ \frac{1}{3} \left| \frac{3\delta\lambda + 2\delta\mu}{\lambda + 2\mu} \right|^2 + \frac{2}{\gamma^2} \left| \frac{\delta\rho}{\rho} \right|^2 + \frac{8}{5} \left| \frac{\delta\mu}{\mu} \right|^2 \right\} \quad (8.15)$$

and

$$\begin{aligned} \sigma_N^s &= \frac{4}{27} \eta \left\{ \left| \frac{\delta\rho}{\rho} \right|^2 (2 + \gamma^2) + \frac{2}{5} \left| \frac{\delta\mu}{\mu} \right|^2 (2\gamma^2 + 3) \right\} \\ &= \sigma_N^{ss} = \frac{8}{27} \eta \left\{ \left| \frac{\delta\rho}{\rho} \right|^2 + \frac{3}{5} \left| \frac{\delta\mu}{\mu} \right|^2 \right\} \end{aligned} \quad (8.16)$$

For the scalar low-contrast case the normalized scattering cross-section may be described by the simple formula (Van der Hulst, 1957)

$$\sigma_N = 2 - \frac{4}{a} \sin a + \frac{4}{a^2} (1 - \cos a) \quad (8.17)$$

where

$$a = 2 \left[1 - \frac{V^{(1)}}{V^{(2)}} \right] \frac{\omega R}{V^{(2)}} \quad (8.18)$$

and where the $V^{(v)}$ are chosen as either $V_p^{(v)}$ or $V_s^{(v)}$, according to the nature of the incident wave. This result can be explained by the interference of the incident and refracted waves propagating in the forward direction, where the parameter a is just the phase difference between these two waves in the far field. Morozhnik (1983a, 1983b) derived this same expression for the low-contrast elastic case. More recently (Korneev and Johnson, 1993b) compared this result with the exact solution for an incident plane P wave and found good agreement for contrasts of about 40%, except at very low frequencies.

It is clear that formula (8.17) is asymptotic to the value 2 in the high-frequency limit. This is the result of the manner in which the problem was formulated, whereby, as mentioned in section 5, the secondary diffracted field contains both the scattered waves and any modifications of the primary incident wave. For the perfectly absorbing sphere, in which case there will not be any waves that are actually scattered, the secondary field U_{sc} must have a value sufficient to cancel the incident wave in the shadow and the normalized scattering cross-section will have an asymptotic value of 1.

9. Low-frequency scattered fields

Expressions (8.1)-(8.5) for the canonical scattering coefficients of a homogeneous elastic sphere may be used to obtain low-frequency asymptotics for the scattered field (4.21). Thus, for the incident P wave (4.22) we have the far field asymptotic solution

$$U_{sc}^P = U_P^P + U_S^P \quad (9.1)$$

$$U_P^P = A \left\{ -\frac{1}{2} \frac{\frac{3}{2}(\lambda_1 - \lambda_2) + \mu_1 - \mu_2}{\frac{1}{2}(\frac{3}{2}\lambda_1 + \mu_1) + \mu_2} + \left(\frac{\rho_1}{\rho_2} - 1 \right) \cos\theta + \frac{2}{3} \left(\frac{\mu_1}{\mu_2} - 1 \right) \frac{\gamma}{D} (1 - 3\cos^2\theta) \right\} \hat{r} \quad (9.2)$$

$$U_S^P = B \left\{ -\left(\frac{\rho_1}{\rho_2} - 1 \right) \sin\theta + \left(\frac{\mu_1}{\mu_2} - 1 \right) \frac{\gamma}{D} \sin 2\theta \right\} \hat{\theta} \quad (9.3)$$

and for the incident S wave (4.24) the far field asymptotic solution has the form

$$U_{sc}^S = U_P^S + U_S^S \quad (9.4)$$

$$U_P^S = A \left\{ \left(\frac{\rho_1}{\rho_2} - 1 \right) \sin\theta - \left(\frac{\mu_1}{\mu_2} - 1 \right) \frac{\gamma}{D} \sin 2\theta \right\} \cos\phi \hat{r} \quad (9.5)$$

$$U_S^S = B \left\{ \left(\frac{\rho_1}{\rho_2} - 1 \right) \cos\theta - \left(\frac{\mu_1}{\mu_2} - 1 \right) \frac{1}{D} \cos 2\theta \right\} \cos\phi \hat{\theta} \\ + B \left\{ -\left(\frac{\rho_1}{\rho_2} - 1 \right) + \left(\frac{\mu_1}{\mu_2} - 1 \right) \frac{1}{D} \cos\theta \right\} \sin\phi \hat{\phi} \quad (9.6)$$

where the following notation has been used

$$A = k_p^2 \frac{V}{4\pi} \frac{e^{-ik_p r}}{r}, \quad B = k_s^2 \frac{V}{4\pi} \frac{e^{-ik_s r}}{r}, \quad V = \frac{4}{3}\pi R^3 \quad (9.7)$$

The case of a low contrast between the material properties of the inclusion and the surrounding material (Born approximation) is defined by the conditions

$$\frac{|\delta\lambda|}{\lambda} = \frac{|\lambda_1 - \lambda_2|}{\lambda_2} \ll 1, \quad \frac{|\delta\mu|}{\mu} = \frac{|\mu_1 - \mu_2|}{\mu_2} \ll 1, \quad \frac{|\delta\rho|}{\rho} = \frac{|\rho_1 - \rho_2|}{\rho_2} \ll 1 \quad (9.8)$$

and then the expressions (9.1)-(9.6) become the same as those obtained by Gubernatis et al. (1977a, 1977b). For an incident P wave these are

$$U_P^P = A \left\{ -\frac{\delta\lambda}{\lambda + 2\mu} + \frac{\delta\rho}{\rho} \cos\theta - \frac{2\delta\mu}{\lambda + 2\mu} \cos^2\theta \right\} \hat{r} \quad (9.9)$$

$$U_S^P = B \left\{ -\frac{\delta\rho}{\rho} \sin\theta + \gamma \frac{\delta\mu}{\mu} \sin 2\theta \right\} \hat{\theta} \quad (9.10)$$

and for an incident S wave they are

$$U_P^S = A \left\{ \frac{\delta\rho}{\rho} \sin\theta - \gamma \frac{\delta\mu}{\mu} \sin 2\theta \right\} \cos\phi \hat{r} \quad (9.11)$$

$$U_S^S = B \left\{ \frac{\delta\rho}{\rho} \cos\theta - \frac{\delta\mu}{\mu} \cos 2\theta \right\} \cos\phi \hat{\theta} + B \left\{ -\frac{\delta\rho}{\rho} + \frac{\delta\mu}{\mu} \cos\theta \right\} \sin\phi \hat{\phi} \quad (9.12)$$

10. Numerical results

In order to illustrate some of the properties of the solutions derived in this paper, numerical calculations were performed for a few sample problems involving a homogeneous spherical inclusion. For the first set of examples the material properties of the surrounding medium were chosen to be representative of a typical continental crust:

$$V_p^{(2)} = 6.0 \text{ km/s}, \quad V_s^{(2)} = 3.5 \text{ km/s}, \quad \rho_2 = 2.7 \text{ g/cm}^3,$$

Five different models were used for the inclusion, with the properties chosen to represent a variety of different types of obstacles that might be encountered in the earth. The elastic parameters for these five models are as follows:

<i>model 1</i>	-	$V_p^{(1)} = 7.5 \text{ km/s}$,	$V_s^{(1)} = 4.4 \text{ km/s}$,	$\rho_1 = 3.1 \text{ g/cm}^3$,
<i>model 2</i>	-	$V_p^{(1)} = 4.5 \text{ km/s}$,	$V_s^{(1)} = 2.6 \text{ km/s}$,	$\rho_1 = 2.3 \text{ g/cm}^3$,
<i>model 3</i>	-	$V_p^{(1)} = 3.4 \text{ km/s}$,	$V_s^{(1)} = 0.0 \text{ km/s}$,	$\rho_1 = 2.7 \text{ g/cm}^3$,
<i>model 4</i>	-	$V_p^{(1)} = 1.4 \text{ km/s}$,	$V_s^{(1)} = 0.0 \text{ km/s}$,	$\rho_1 = 1.0 \text{ g/cm}^3$,
<i>model 5</i>	-	$V_p^{(1)} = 0.0 \text{ km/s}$,	$V_s^{(1)} = 0.0 \text{ km/s}$,	$\rho_1 = 0.0 \text{ g/cm}^3$,

For each of these models the scattering problem was solved for an incident plane P wave and also for an incident plane S wave. The results of the calculations are presented by plotting the normalized scattering cross-sections σ_N^P and σ_N^S as a function of the parameter $\xi = \xi_2 = \omega R / V_p^{(2)}$.

Models 1 and 2 simulate high-velocity and low-velocity inclusions, respectively, with the difference in material properties being about 20% in each case. Figures 1 (model 1) and 2 (model 2) present the normalized cross sections for these two types of inclusions. The general pattern of the total scattered field in these cross sections is described by an increase as ω^4 at low frequencies which merges into long large oscillations about a constant value of 2.0 at higher frequencies. These long oscillations are caused by the interference between the waves that propagate through the inclusion and those that propagate around it (Van der Hulst, 1957), and the asymptotic value of 2.0, as discussed earlier, results

from the fact that the scattered field contains both the waves scattered by the inclusion and the disturbance of the primary field. Superimposed on this pattern, particularly evident in Figure 2, are some short small amplitude oscillations caused by multiple reflections within the inclusion. Because the low-velocity inclusion tends to focus energy within the obstacle much more than the high-velocity inclusion, these short oscillations are much more pronounced for the low-velocity inclusion.

Of particular interest in Figures 1 and 2 is the comparison of the scattering cross sections for incident P waves and S waves at low frequencies where the wavelengths are larger than the size of the scatterer. In this frequency range the $P \rightarrow S$ scattering is much stronger than the $S \rightarrow P$ scattering, in agreement with the results derived in section 7. For an incident P wave the energy scattered into the S field can exceed that scattered into the P field, whereas in the case of the incident S wave the amount of energy scattered into the P field is negligible compared to that scattered into the S field.

Models 3 and 4 are fluid inclusions, with model 3 simulating an inclusion of molten rock and model 4 simulating an inclusion filled with water. The scattering cross sections for these fluid inclusions are plotted in Figures 3 and 4 and show a pattern similar to that of the elastic inclusions except that all of the features are shifted toward lower frequencies. Because of this, the scattering reaches significant levels at rather low frequencies where the size of the inclusion is still much smaller than the wavelength of the incident wave. The observation made for the elastic inclusions that the $P \rightarrow S$ scattering is much stronger than the $S \rightarrow P$ scattering is even more pronounced for the fluid inclusions, with the scattered S field dominating the scattered P field at low frequencies regardless of whether the incident field is a P wave or S wave. In addition, for the case of the incident P wave the scattered S field is now comparable to the scattered P field over the entire frequency range.

For the case of the water filled inclusion (Figure 4) the resonant features of the scattering cross sections are particularly conspicuous. The positions of the resonance peaks correspond to the real parts of the complex roots of the determinant (A.9) contained in the denominator of the canonical scattering coefficients. Some of these roots (including the first one) may be obtained by letting $l = 1$ in (A.9), which leads to the equation

$$j_2(\xi_1) - \frac{j_1(\xi_1)}{\xi_1} = 0, \quad \xi_1 = \frac{\omega R}{V_p^{(1)}} \quad (10.1)$$

The first few roots of this equation are $\xi_1 \approx 2.1, 5.9, 9.2, \dots$.

In model 5 the inclusion is a hollow cavity and the scattering cross sections are shown in Figure 5. It is useful to think of this model as a modification of the water-filled inclusion of model 4 in which $V_p^{(1)}$ and ρ_1 are reduced to zero. This helps explain why the scattering cross sections of Figure 5 are

essentially smoothed versions of those in Figure 4, with the main differences being related to the fact that the cavity has no resonances associated with the scattered field within the inclusion. The fact that the general patterns of the scattering cross sections in Figures 4 and 5 are similar indicates that this pattern is controlled primarily by the vanishing of the shear modulus within the inclusion.

It is worth pointing out that the properties of the material surrounding the inclusion and wavelengths of the incident waves are identical in the Figures 1-5. However, it is clear that the common features of the scattering cross sections are found at rather different frequencies for the different types of inclusions. This result can be explained if one describes the frequency dependence of the scattering cross sections in terms of the wavelength of the scattered field rather than the wavelength of the incident wave. Note that in applying this reasoning, the wavelengths of the scattered fields both inside and outside the inclusion must be considered. This general principle explains why the scattering cross sections of the S field is always shifted toward lower frequencies with respect to those of the P field (compare the upper and lower panels in Figures 1, 2, and 3), why low-velocity inclusions have scattering cross sections that are shifted toward low frequencies with respect to those of high-velocity inclusions (compare Figures 1, 2, 3, 4, and 5), and why the position of the resonance peaks in the scattering cross sections depend upon the velocity within the inclusion (compare Figures 3 and 4).

This same type of reasoning about the wavelength of the scattered field also helps explain the general result that the $P \rightarrow S$ scattering is stronger than the $S \rightarrow P$ scattering at low frequencies. From section 9 it is clear that the low-frequency scattering energy is proportional to $(R/\text{wavelength})^4$. Such a result favors the scattering of S waves because of their shorter wavelength. Another way of saying this is that, using the scale of wavelengths, an inclusion appears larger to an S wave than to a P wave and thus it is scattered more intensively. What is not so obvious is that the ratio in the scattering intensities for the converted waves should be independent of frequency and proportional to the squared ratio of the velocities. However, it is clear in Figures 1 - 5 that the shape of σ_N^{PS} curve is always identical to the corresponding σ_N^{SP} curve, with the amplitudes of the curves scaled according to (7.1).

In Section 8 it was pointed out that the case of an inclusion with intrinsic attenuation can be treated by assigning complex values to the elastic parameters within the inclusion. Examples of the normalized scattering cross sections for this type of an inclusion are shown in Figures 6 and 7. The attenuation was characterized in terms of the quality factor Q_1 where

$$Q_1^{-1} = \frac{\text{Im}\{\lambda_1\}}{\text{Re}\{\lambda_1\}} = \frac{\text{Im}\{\mu_1\}}{\text{Re}\{\mu_1\}} \quad (10.1)$$

The calculations were performed for the low frequency case where $k_p R = 0.05$ and the figures show

how the cross section changes as the attenuation of the inclusion is increased. Figure 6 shows the results for the high-velocity inclusion listed earlier as model 1, and Figure 7 is for the low-velocity inclusion of model 2. The results are quite similar for the two types of inclusions. For small attenuation the scattering cross sections are just the low frequency values shown in Figures 1 and 2. As the attenuation is increased the scattering cross sections also increase and approach the limiting values associated with the coefficients given in (8.9) and (8.10). The attenuation affects the scattered S waves much more than the scattered P waves, as the scattering cross sections for the incident S wave reaches values which are about 3 times those for the incident P wave. Furthermore, for both cases of an incident P wave and an incident S wave the scattered field consists almost entirely of S waves.

The basic solutions presented in this paper are completely general in that they can be applied over the entire frequency range and to an inclusion of any size. For instance, the scattering cross sections of Figure 3 can be used to provide a rough estimate of scattering by the earth's fluid core. More appropriate results can be obtained by choosing the following material properties to represent the earth's mantle and outer core:

$$V_p^{(2)} = 11.3 \text{ km/s} , \quad V_s^{(2)} = 6.2 \text{ km/s} , \quad \rho_2 = 5.0 \text{ gm/cm}^3$$

$$V_p^{(1)} = 9.9 \text{ km/s} , \quad V_s^{(1)} = 0.0 \text{ km/s} , \quad \rho_1 = 6.0 \text{ gm/cm}^3$$

These velocities were chosen to match the average travel times through the mantle and core, and the densities were chosen to match the contrast in acoustic impedance at the mantle-core boundary. The radius of the core was taken as 3482 km. For this example it is instructive to consider the complete solutions to the scattering problem in the time domain. The expansion coefficients for the incident field of (4.14) were chosen to represent a point pressure source at a radius of 6300 km, and then the scattered field of (4.21) was evaluated and transformed from the frequency domain to the time domain. (Korneev and Johnson (1993a) show how the solution for a point source is easily obtained from the plane wave solutions.) The spectrum of the pressure at the source was flat below a corner frequency corresponding to a period of 30 sec. The total solutions, including both the incident and scattered fields, are shown in Figure 8 at 6-degree angular intervals for a radius of 6371 km. Note that this is an example of high-frequency scattering, as $k_p R$ has a value of 730.

There are a variety of interesting features on the seismograms of Figure 8, but the discussion here will concentrate primarily upon some of the diffraction effects. A good example of this is the arrivals that fill in the gap between the PcS and PKS phases. The geometrical ray arrivals for the PcS wave end at a distance of 72 degrees and those of the PKS wave begin at 122 degrees, but in Figure 8 this gap is completely filled by diffracted waves. Another example is the P2KS phase which ends with a

caustic at a distance of 175 degrees, but strong diffracted waves extend out to 180 degrees and back to less than 150 degrees where they merge with the PKS phase. The situation is actually more complicated than this, as the P3KS geometrical arrival extends out to 115 degrees and then is continued by diffracted waves that merge with the P2KS wave near 180 degrees, while the P4KS geometrical arrival extends to 55 degrees and is continued by diffracted waves near 100 degrees. Thus the waves P4KS, P3KS, P2KS, PKS and PcS along with their diffractions all come together to form a complex and continuous group of waves that appear on these seismograms between a distance of 60 degrees and time of 2300 seconds, extend out to 180 degrees and 1600 seconds, and then continue back to a distance of 0 degrees and 700 seconds. Increasing the amplitude of the seismograms would allow this same type of pattern to be extended to include the P5KS wave and other higher order core waves of this family. The same type of phenomenon also occurs for the PKP family of waves, although these waves are of slightly lower amplitude than the PKS waves and thus not as easily observed in Figure 8.

The distances mentioned above for the regions of geometrical arrivals and diffracted waves will be slightly different in the real earth because of the radial variation in velocity in the mantle and core. The seismograms will also be considerably more complicated because of the additional waves caused by the inner core, the surface of the earth, and S waves generated at the source in the case of earthquakes. However, the relative amplitudes of the different waves, the distortions in the waveforms, and the interaction between the geometrical and diffracted arrivals shown in Figure 8 should be generally applicable to long period waves in the earth.

There is one other feature present in Figure 8 which is worth mentioning. On the radial component at a distance of 180 degrees and at a time of about 2500 sec there is just discernible a long period wave (period of about 600 sec). This is an interface wave of the Stonely or Scholte type which travels on the mantle-core boundary with a velocity of about 4.4 km/sec.

11. Discussion and conclusions

The primary purpose of this paper is to present in a convenient form the exact solutions for the scattering of P waves and S waves by a spherical inclusion and to point out some of the important properties of this solution. However, it is also worth considering whether these results can be used to make some general inferences about the scattering of elastic waves in the earth. In doing this the first point which must be discussed is the applicability of results for a spherical inclusion to the situation in the earth where the shape of the inclusion is often unknown, but most likely different from that of an exact sphere. Here one can appeal to the fact that scattering by a sphere represents a canonical problem

for a more extended class of objects with relatively simple and smooth boundaries, and thus reason that these results should apply in an approximate manner to a wide class of objects having these properties. In the low-frequency range (Rayleigh scattering) an even stronger argument is possible, as it was shown in section 9 that for this case the solutions depend only upon the volume of the inclusion and not upon its shape. Thus the low frequency results presented in this paper should be applicable to small 3D inclusions of any shape in the earth.

In the low-frequency range there is a strong asymmetry in the relative scattering of P waves and S waves. The $P \rightarrow S$ scattering is generally much more intensive than the $S \rightarrow P$ scattering. This is explained in a qualitative sense by the fact that the inclusion appears to be larger to the S wave because of its shorter wavelength, and the fact that the scattering is controlled by the wavelength of the scattered wave rather than the wavelength of the incident wave. It is common for an incident P wave to have more energy in the scattered S field than the scattered P field, whereas for an incident S wave almost all of the scattered energy is in the S field. This suggests that the coda of P waves should contain a significant proportion of S waves, while the coda of S waves should be predominantly S waves.

This asymmetry in the scattering conversion of P and S waves can be quantified for the case of the spherically symmetric scatterers considered in this paper. It was shown in section 7 that the mean intensity of the $P \rightarrow S$ converted waves is $2V_p^4/V_s^4$ times the mean intensity of the $S \rightarrow P$ converted waves, and this ratio is independent of frequency. For more general scatterers it is possible to write reciprocal relations such as those given in Appendix D, but it is not obvious how these can be converted to intensity ratios such as that just given for a spherical scatterer. However, at low frequencies in the domain of Rayleigh scattering where only the volume of the inclusion is important, it is conjectured that the ratio of the mean intensities of the converted waves will approach the value obtained for spherical scatterers. Thus this strong asymmetry in the scattering conversion of P and S waves is likely to be a general result when the wavelengths are large compared to the size of the inclusion.

The scattering from a fluid inclusion is more intensive than the scattering from an elastic inclusion, with the general frequency dependence of the scattering being controlled by the contrast in the shear modulus. Superimposed upon this frequency dependence is a series of resonance peaks which are controlled by compressional velocity of the fluid. There exists the potential here to use the spectrum of the scattered waves to estimate the dimensions of the scatterers, although the case where there is a distribution in the size of the scatterers would tend to smooth out the resonance peaks. Regardless, the amount of energy scattered into the S field by an incident P wave is an effective diagnostic which can be used over the entire frequency range to identify fluid inclusions.

In the case of a low contrast between the material properties of the inclusion and the surrounding medium only a few of the scattering coefficients need be included in the low-frequency range and they have a simple dependence upon the material properties (equations (8.1)-(8.5)). The form of these coefficients is suitable for use in inverse problems, with some of the coefficients depending primarily upon the contrast in density, others depending primarily upon the contrast in shear modulus, and others depending upon the contrast in compressibility.

One feature of the low-contrast approximation, as is true of most Born-type approximations, is that it does not satisfy conservation of energy. However, this is easily remedied. The equations (5.8)-(5.10) are derived from (5.2) and are essentially statements of conservation of energy. The right-hand sides of these equations, which involve only the real parts of the canonical scattering coefficients, represent the energy terms that are coherent with the primary field and thus account for the change in energy of the primary field that must occur when additional scattered fields are generated. Applying this to the low-contrast case, we note that the coefficients (8.1)-(8.6) are completely imaginary and represent only the scattered fields, the real parts which represent the change in the primary field having been dropped in the approximation. However, these real parts can be recovered from the expressions (5.8)-(5.10), and including the real parts will restore the conservation of energy. Note that because the coefficients (8.1)-(8.6) all have an $(\omega)^3$ frequency dependence, the real parts of these coefficients will have an $(\omega)^6$ frequency dependence, which in most cases will make them small enough to be neglected. However, in some situations, such as studies of attenuation of primary waves due to scattering, these real parts of the scattering coefficients should be included in order to achieve a formulation more compatible with energy conservation.

A caveat involving intrinsic attenuation should be mentioned here. As mentioned in section 8, the canonical scattering coefficients can be modified to include intrinsic attenuation by introducing complex elastic parameters. However, in this case some of the relations, including (5.8)-(5.11), are no longer valid because strain energy is no longer conserved. The analysis of the low-contrast approximation is still possible, as introducing complex elastic parameters into (8.1)-(8.6) produces real parts of these coefficients which are proportional to $(\omega)^3$ and which cause an attenuation of the primary field due to the intrinsic attenuation which dominates that due to the scattering.

Appendix A

Consider the case of a homogeneous elastic sphere of radius R with elastic parameters λ_1 , μ_1 and density ρ_1 surrounded by a medium having elastic parameters λ_2 , μ_2 , and density ρ_2 with the continuous boundary conditions (4.17). The canonical scattering coefficients have the following analytical representations.

$$a_l^{PP} = \frac{\Delta_{PP}}{\Delta}, \quad b_l^{PS} = \frac{\Delta_{PS}}{\Delta}, \quad a_l^{SP} = \frac{\Delta_{SP}}{\Delta}, \quad b_l^{XS} = \frac{\Delta_{SS}}{\Delta} \quad (\text{A.1})$$

$$c_l^S = - \frac{\frac{\mu_1}{\mu_2} \eta_l j_{l-1}(\eta_1) j_l(\eta_2) - \eta_l j_l(\eta_1) j_{l-1}(\eta_2) + (l+2) \left[1 - \frac{\mu_1}{\mu_2} \right] j_l(\eta_1) j_l(\eta_2)}{\frac{\mu_1}{\mu_2} \eta_l j_{l-1}(\eta_1) h_l(\eta_2) - \eta_l j_l(\eta_1) h_{l-1}(\eta_2) + (l+2) \left[1 - \frac{\mu_1}{\mu_2} \right] j_l(\eta_1) h_l(\eta_2)} \quad (\text{A.2})$$

where

$$\begin{aligned} \Delta = & \frac{(\eta_2 \xi_2)^3}{(2l+1)^2} \left\{ \frac{h_l(\xi_2)}{\xi_2} \frac{h_l(\eta_2)}{\eta_2} (2l+1) \Delta_1 + \frac{j_l(\xi_1)}{\xi_1} \frac{j_l(\eta_1)}{\eta_1} (2l+1) \Delta_2 \left[\frac{\rho_1}{\rho_2} \right]^2 \right. \\ & - (2l+1) \frac{\rho_1}{\rho_2} \left[\frac{h_l(\xi_2)}{\xi_2} \frac{j_l(\eta_1)}{\eta_1} \Delta_{12} + \frac{j_l(\xi_1)}{\xi_1} \frac{h_l(\eta_2)}{\eta_2} \Delta_{21} \right] \\ & - q \Delta_1 \left[\Delta_2 + (l+2) h_{l+1}(\xi_2) h_{l+1}(\eta_2) + (l-1) h_{l-1}(\xi_2) h_{l-1}(\eta_2) \right] \\ & \left. + q \frac{\rho_1}{\rho_2} \Delta_2 \left[\Delta_1 + (l+2) j_{l+1}(\xi_1) j_{l+1}(\eta_1) + (l-1) j_{l-1}(\xi_1) j_{l-1}(\eta_1) \right] + q^2 (l-1)(l+2) \Delta_1 \Delta_2 \right\} \quad (\text{A.3}) \end{aligned}$$

$$\begin{aligned} \Delta_{PS} = & i \frac{\eta_2^5}{2l+1} \left\{ \frac{\Delta_1}{2l+1} q \left[(l-1)(l+2)q-1 \right] - \frac{j_l(\xi_1)}{\xi_1} \frac{j_l(\eta_1)}{\eta_1} \frac{\rho_1}{\rho_2} \left[1 - \frac{\rho_1}{\rho_2} - (l+2)(2l+1)q \right] \right. \\ & \left. + q \frac{\rho_1}{\rho_2} \left[2j_{l+1}(\xi_1) \frac{j_l(\eta_1)}{\eta_1} + j_{l+1}(\eta_1) \frac{j_l(\xi_1)}{\xi_1} \right] \right\} \quad (\text{A.4}) \end{aligned}$$

$$\Delta_{SP} = \gamma_2^3 l(l+1) \Delta_{PS} \quad (\text{A.5})$$

An expression for Δ_{PP} can be derived from (A.3) by substituting for the functions $h_k(\xi_2)$ ($k = l-1, l, l+1$) the corresponding functions $-j_k(\xi_2)$. Analogously, Δ_{SS} can be derived from the same expression by substituting for the functions $h_k(\eta_2)$ ($k = l-1, l, l+1$) the corresponding functions $-j_k(\eta_2)$. The following definitions have been used in equations (A.2)-(A.5).

$$\begin{aligned} \Delta_1 &= (l+1) j_{l+1}(\xi_1) j_{l-1}(\eta_1) + l j_{l-1}(\xi_1) j_{l+1}(\eta_1) \\ \Delta_2 &= (l+1) h_{l+1}(\xi_2) h_{l-1}(\eta_2) + l h_{l-1}(\xi_2) h_{l+1}(\eta_2) \\ \Delta_{12} &= (l+1) j_{l+1}(\xi_1) h_{l-1}(\eta_2) + l j_{l-1}(\xi_1) h_{l+1}(\eta_2) \\ \Delta_{21} &= (l+1) h_{l+1}(\xi_2) j_{l-1}(\eta_1) + l h_{l-1}(\xi_2) j_{l+1}(\eta_1) \end{aligned} \quad (\text{A.6})$$

$$q = \frac{2}{\eta_2^2} \left[1 - \frac{\rho_1 \eta_2^2}{\rho_2 \eta_1^2} \right] = \frac{2}{\eta_2^2} \left[1 - \frac{\mu_1}{\mu_2} \right], \quad \gamma_2 = \frac{V_s^{(2)}}{V_p^{(2)}}$$

$$\xi_1 = \frac{\omega R}{V_p^{(1)}}, \quad \eta_1 = \frac{\omega R}{V_s^{(1)}}, \quad V_p^{(1)} = \sqrt{\frac{\lambda_1 + 2\mu_1}{\rho_1}}, \quad V_s^{(1)} = \sqrt{\frac{\mu_1}{\rho_1}} \quad (\text{A.7})$$

$$\xi_2 = \frac{\omega R}{V_p^{(2)}}, \quad \eta_2 = \frac{\omega R}{V_s^{(2)}}, \quad V_p^{(2)} = \sqrt{\frac{\lambda_2 + 2\mu_2}{\rho_1}}, \quad V_s^{(2)} = \sqrt{\frac{\mu_2}{\rho_2}}$$

For the case of a fluid within the sphere ($\mu_1 = 0$), the above expressions reduce to

$$c_l^s = -\frac{(l+2)j_l(\eta_2) - \eta_2 j_{l-1}(\eta_2)}{(l+2)h_l(\eta_2) - \eta_2 h_{l-1}(\eta_2)} \quad (\text{A.8})$$

$$\Delta = \frac{\eta_2^3 \xi_2^3}{2l+1} \left\{ (2l+1) \frac{h_l(\xi_2)}{\xi_2} h_l(\eta_2) \left[j_{l+1}(\xi_1) - \frac{l}{\xi_1} j_l(\xi_1) \right] \right. \\ \left. - (2l+1) \frac{\rho_1}{\rho_2} \frac{j_l(\xi_1)}{\xi_1} h_l(\eta_2) \left[h_{l+1}(\xi_2) - \frac{l}{\xi_2} h_l(\xi_2) \right] \right. \\ \left. - \frac{2}{\eta_2} \left[j_{l+1}(\xi_1) - \frac{l}{\xi_1} j_l(\xi_1) \right] \left[\Delta_2 + (l+2)h_{l+1}(\xi_2)h_{l+1}(\eta_2) + (l-1)h_{l-1}(\xi_2)h_{l-1}(\eta_2) \right] \right. \\ \left. + \frac{2}{\eta_2} \frac{\rho_1}{\rho_2} \Delta_2 \left[2j_{l+1}(\xi_1) - \frac{2l-1}{\xi_1} j_l(\xi_1) \right] + \frac{4}{\eta_2^3} (l-1)(l+2) \Delta_2 \left[j_{l+1}(\xi_1) - \frac{l}{\xi_1} j_l(\xi_1) \right] \right\} \quad (\text{A.9})$$

$$\Delta_{ps} = 2 \frac{\eta_2^3}{2l+1} \left\{ \left[j_{l+1}(\xi_1) - \frac{l}{\xi_1} j_l(\xi_1) \right] \left[1 - (l-1)(l+2) \frac{2}{\eta_2^2} \right] + \frac{j_l(\xi_1)}{\xi_1} \frac{\rho_1}{\rho_2} \right\} \quad (\text{A.10})$$

$$\Delta_{sp} = \gamma_2^3 l(l+1) \Delta_{ps} \quad (\text{A.11})$$

Expressions for Δ_{pp} and for Δ_{ss} can be derived from Δ in the same way as in the elastic case.

For the case of a cavity the above expressions can be further simplified to

$$c_l^s = -\frac{(l+2)j_l(\eta_2) - \eta_2 j_{l-1}(\eta_2)}{(l+2)h_l(\eta_2) - \eta_2 h_{l-1}(\eta_2)} \quad (\text{A.12})$$

$$\Delta = \eta_2^3 \xi_2^3 \left\{ \frac{h_l(\xi_2)}{\xi_2} h_l(\eta_2) + \frac{4(l-1)(l+2)\Delta_2}{(2l+1)\eta_2^3} \right. \\ \left. - \frac{2}{\eta_2} \left[\Delta_2 + (l+2)h_{l+1}(\xi_2)h_{l+1}(\eta_2) + (l-1)h_{l-1}(\xi_2)h_{l-1}(\eta_2) \right] \right\} \quad (\text{A.13})$$

$$\Delta_{ps} = 2i \frac{\eta_2^3}{2l+1} \left[1 - (l-1)(l+2) \frac{2}{\eta_2^2} \right] \quad (\text{A.14})$$

$$\Delta_{SP} = \gamma_2^3 l(l+1) \Delta_{PS} \quad (\text{A.15})$$

Expressions for Δ_{PP} and for Δ_{SS} can be derived from Δ in the same manner as in the previous cases.

Appendix B

The diffracted field inside a homogeneous elastic sphere may be calculated using the expression (4.21), where all of the spherical Hankel functions h_k are replaced by spherical Bessel functions j_k and where the wavenumbers k_p and k_s are taken for the inner medium $v = 1$. The canonical scattering coefficients for the inner medium have the forms

$$a_l^{PP} = \frac{\Delta_{PP}}{\Delta}, \quad b_l^{PS} = \frac{\Delta_{PS}}{\Delta}, \quad a_l^{SP} = \frac{\Delta_{SP}}{\Delta}, \quad b_l^{SS} = \frac{\Delta_{SS}}{\Delta} \quad (\text{B.1})$$

$$c_l^S = i \left[\frac{\mu_1}{\mu_2} \eta_1 \eta_2 j_{l-1}(\eta_1) h_l(\eta_2) - \eta_2^2 j_l(\eta_1) h_{l-1}(\eta_2) + (l+2) \eta_2 \left[1 - \frac{\mu_1}{\mu_2} \right] j_l(\eta_1) h_l(\eta_2) \right]^{-1} \quad (\text{B.2})$$

with

$$\Delta_{PP} = i \frac{\eta_2^5}{2l+1} \left\{ \frac{h_l(\eta_2)}{\eta_2} \left[l \left[1 - \frac{\rho_1}{\rho_2} - (l+2)(2l+1)q \right] \frac{j_l(\eta_1)}{\eta_1} + (l(l+2)q-1) j_{l-1}(\eta_1) \right] + h_{l-1}(\eta_2) \left[\left[\frac{\rho_1}{\rho_2} + l(l+2)q \right] \frac{j_l(\eta_1)}{\eta_1} - q j_{l-1}(\eta_1) \right] \right\} \quad (\text{B.3})$$

$$\Delta_{PS} = -i \frac{\eta_2^5}{2l+1} \left\{ \frac{h_l(\eta_2)}{\eta_2} \left[\left[1 - \frac{\rho_1}{\rho_2} - (l+2)(2l+1)q \right] \frac{j_l(\xi_1)}{\xi_1} + (l+2)q j_{l-1}(\xi_1) \right] + h_{l-1}(\eta_2) q \left[(l+2) \frac{j_l(\xi_1)}{\xi_1} - j_{l-1}(\xi_1) \right] \right\} \quad (\text{B.4})$$

$$\Delta_{SP} = i \frac{l(l+1)}{(2l+1)^2} \xi_2^3 \left\{ 2 \left[(l+2) h_{l+1}(\xi_2) j_{l+1}(\eta_1) + (l-1) h_{l-1}(\xi_2) j_{l-1}(\eta_1) \right] \left[1 - \frac{\mu_1}{\mu_2} \right] - (2l+1) \eta_2^2 \frac{j_l(\eta_1)}{\eta_1} \frac{h_l(\xi_2)}{\xi_2} \left[1 - \frac{\rho_1}{\rho_2} \right] \right\} \quad (\text{B.5})$$

$$\Delta_{SS} = i \frac{\xi_2^3}{(2l+1)^2} \left\{ (l+1)(2l+1) \eta_2^2 \frac{j_l(\xi_1)}{\xi_1} \frac{h_l(\xi_2)}{\xi_2} \left[1 - \frac{\rho_1}{\rho_2} \right] - (2l+1) \frac{\eta_2^2}{\xi_2} \left[h_l(\xi_2) j_{l-1}(\xi_1) - \frac{\rho_1}{\rho_2} \frac{\xi_2}{\xi_1} h_{l-1}(\xi_2) j_l(\xi_1) \right] - 2 \left[(l+1)(l+2) h_{l+1}(\xi_2) j_{l+1}(\xi_1) - l(l-1) h_{l-1}(\xi_2) j_{l-1}(\xi_1) \right] \left[1 - \frac{\mu_1}{\mu_2} \right] \right\} \quad (\text{B.6})$$

where the expression for Δ is given by (A.3) and the notation (A.6) has been used.

For the case of a fluid within the sphere, the above expressions can be reduced to

$$c_l^S = 0 \quad (\text{B.7})$$

$$\Delta_{PP} = i \frac{\eta_2^4}{2l+1} \left\{ h_l(\eta_2) + \frac{2}{\eta_2} \left[(l^2-1) \frac{h_l(\eta_2)}{\eta_2} - h_{l+1}(\eta_2) \right] \right\} \quad (\text{B.8})$$

$$\Delta_{PS} = 0 \quad (\text{B.9})$$

$$\Delta_{SP} = i \xi_2^3 \frac{2l(l+1)}{(2l+1)} \left[h_{l+1}(\xi_2) - (l-1) \frac{h_l(\xi_2)}{\xi_2} \right] \quad (\text{B.10})$$

$$\Delta_{SS} = 0 \quad (\text{B.11})$$

where the expressions for Δ is given by (A.9).

Appendix C

For the case of the incident plane P wave (4.22) the scattered field in the outer medium has the form

$$\begin{aligned} \mathbf{U}_{sc} &= \mathbf{U}_{PP} + \mathbf{U}_{PS} = \sum_{l \geq 0} \left\{ \left[a_l^{PP} h_{l+1}(k_p r) + l b_l^{PS} h_{l+1}(k_s r) \right] \mathbf{Y}_{l0}^+ \right. \\ &\quad \left. + \left[-a_l^{PP} h_{l-1}(k_p r) + (l+1) b_l^{PS} h_{l-1}(k_s r) \right] \mathbf{Y}_{l0}^- \right\} e^{-i \frac{\pi}{2} (l+1)} \\ &= \sum_{l \geq 0} e^{-i \frac{\pi}{2} (l+1)} (2l+1) \left\{ a_l^{PP} \left[\left[(l+1) \frac{h_l(k_p r)}{k_p r} - h_{l-1}(k_p r) \right] P_l(\cos \theta) \hat{\mathbf{e}} - \frac{h_l(k_p r)}{k_p r} \frac{\partial P_l(\cos \theta)}{\partial \theta} \hat{\boldsymbol{\theta}} \right] \right. \\ &\quad \left. + b_l^{PS} \left[l(l+1) \frac{h_l(k_s r)}{k_s r} P_l(\cos \theta) \hat{\mathbf{e}} + \left[h_{l-1}(k_s r) - \frac{h_l(k_s r)}{k_s r} \right] \frac{\partial P_l(\cos \theta)}{\partial \theta} \hat{\boldsymbol{\theta}} \right] \right\} \quad (\text{C.1}) \end{aligned}$$

For the case of the incident plane S wave (4.24) the scattered field in the outer medium has the form

$$\begin{aligned} \mathbf{U}_{sc} &= \mathbf{U}_{PS} + \mathbf{U}_{SS} = \sum_{l, m} \left\{ c_{lm}^0 c_l^S h_l(k_s r) \mathbf{Y}_{lm}^0 + \left[b_{lm}^0 a_l^{SP} h_{l+1}(k_p r) + l b_{lm}^0 b_l^{SS} h_{l+1}(k_s r) \right] \mathbf{Y}_{lm}^+ \right. \\ &\quad \left. + \left[-b_{lm}^0 a_l^{SP} h_{l-1}(k_p r) + (l+1) b_{lm}^0 b_l^{SS} h_{l-1}(k_s r) \right] \mathbf{Y}_{lm}^- \right\} \quad (\text{C.2}) \end{aligned}$$

in terms of the spherical vectors (3.1), and

$$\mathbf{U}_{sc} = \mathbf{U}_{PS} + \mathbf{U}_{SS}$$

$$\begin{aligned}
&= \sum_{l \geq 1} e^{-i\frac{\pi}{2}(l+1)} \frac{(2l+1)}{2l(l+1)} \left[2 \cos \phi \left[a_l^{SP} \left[h_{l-1}(k_p r) - (l+1) \frac{h_l(k_p r)}{k_p r} \right] - b_l^{SS} l(l+1) \frac{h_l(k_s r)}{k_s r} \right] P_l^1(\cos \theta) \hat{r} \right. \\
&+ \cos \phi \left[i c_l^{SS} Q_1(\theta) h_l(k_s r) + a_l^{SP} Q_2(\theta) \frac{h_l(k_p r)}{k_p r} + b_l^{SS} Q_2(\theta) \left[l \frac{h_l(k_s r)}{k_s r} - h_{l-1}(k_s r) \right] \right] \hat{\theta} \\
&+ \left. \sin \phi \left[c_l^{SS} Q_2(\theta) h_l(k_s r) + i a_l^{SP} Q_1(\theta) \frac{h_l(k_p r)}{k_p r} + i b_l^{SS} Q_1(\theta) \left[l \frac{h_l(k_s r)}{k_s r} - h_{l-1}(k_s r) \right] \right] \hat{\phi} \right] \quad (C.3)
\end{aligned}$$

in a spherical coordinate system, where

$$\begin{aligned}
b_{lm}^0 &= \frac{1}{2l(l+1)} \left[l(l+1) \delta_{m,-1} - \delta_{m,1} \right] e^{-i\frac{\pi}{2}(l+1)} \\
c_{lm}^0 &= -\frac{2l+1}{2l(l+1)} \left[l(l+1) \delta_{m,-1} + \delta_{m,1} \right] e^{-i\frac{\pi}{2}(l+1)} \\
Q_1(\theta) &= P_{l-1}^2(\cos \theta) + l(l+1) P_{l-1}^0(\cos \theta), \quad Q_2(\theta) = l(l+1) P_l^0(\cos \theta) - P_l^2(\cos \theta)
\end{aligned}$$

Appendix D

The purpose of this appendix is to extend the analysis of Aki (1982) to the case of P and S waves having arbitrary polarizations. Consider a localized scatterer with a spherical coordinate system centered upon it. At the point (r, θ_1, ϕ_1) is located the unit radial force

$$f_P(r, \theta_1, \phi_1) = \hat{r} \quad (D.1)$$

The scattered S wave generated by this force and observed at a second location (r, θ_2, ϕ_2) is

$$\begin{aligned}
u_{PS}(r, \theta_2, \phi_2) &= u_{PS1}(r, \theta_2, \phi_2) \hat{\theta} + u_{PS2}(r, \theta_2, \phi_2) \hat{\phi} \\
&= u_{PS}(r, \theta_2, \phi_2) \{ (\cos \alpha_2) \hat{\theta} + (\sin \alpha_2) \hat{\phi} \}
\end{aligned} \quad (D.2)$$

where α_2 is the polarization angle of the S wave at the second location. It has been assumed here that the distance r is sufficiently large so that only far field parts of the solution need be included. At this second location two separate forces are considered. The first is the unit transverse force

$$f_{S1}(r, \theta_2, \phi_2) = \hat{\theta} \quad (D.3)$$

At the first location (r, θ_1, ϕ_1) this gives rise to a scattered P wave with displacement

$$u_{S1P}(r, \theta_1, \phi_1) = u_{S1P}(r, \theta_1, \phi_1) \hat{r} \quad (D.4)$$

The reciprocal theorem states that

$$f_P(r, \theta_1, \phi_1) \cdot u_{S1P}(r, \theta_1, \phi_1) = f_{S1}(r, \theta_2, \phi_2) \cdot u_{PS}(r, \theta_2, \phi_2) \quad (D.5)$$

and in the present case, using (D.1-D.4), this means that

$$u_{S1P}(r, \theta_1, \phi_1) = u_{PS1}(r, \theta_2, \phi_2) \quad (D.6)$$

The second force to be considered is the unit transverse force

$$f_{S2}(r, \theta_2, \phi_2) = \hat{\phi} \quad (D.7)$$

which produces a P wave at the first location with displacement

$$u_{S2P}(r, \theta_1, \phi_1) = u_{S2P}(r, \theta_1, \phi_1) \hat{r} \quad (D.8)$$

Applying the reciprocal theorem in this case yields

$$u_{S2P}(r, \theta_1, \phi_1) = u_{PS2}(r, \theta_2, \phi_2) \quad (D.9)$$

The two expressions (D.6) and (D.9) are the reciprocal relations for two orthogonal polarizations of the S wave. In general both polarizations will be present in a scattered P wave and thus both reciprocal relations are required.

In the vicinity of the scatterer the amplitude of the P wave incident from the first location will be

$$u_P^{(i)} = \frac{1}{4\pi\rho V_P^2 r}$$

and that of both S waves incident from the second location will be

$$u_S^{(i)} = \frac{1}{4\pi\rho V_S^2 r}$$

Thus (D.6) can be written in terms of amplitude ratios as

$$\frac{u_{S1P}(r, \theta_1, \phi_1)}{u_S^{(i)}} = \frac{V_S^2}{V_P^2} \frac{u_{PS1}(r, \theta_2, \phi_2)}{u_P^{(i)}} \quad (D.10)$$

and (D.9) becomes

$$\frac{u_{S2P}(r, \theta_1, \phi_1)}{u_S^{(i)}} = \frac{V_S^2}{V_P^2} \frac{u_{PS2}(r, \theta_2, \phi_2)}{u_P^{(i)}} \quad (D.11)$$

These are exact relationships for the two polarizations of the S wave and they show that in each case the $P \rightarrow S$ scattering is stronger than the $S \rightarrow P$ scattering by a factor of $(V_P/V_S)^2$. The result (D.10) with $\phi_1 = \phi_2 = 0$ is essentially that derived by Aki (1992). While these results are very general, they are not entirely suited to the scattering problem. First, they deal only with the separate components of the motion and cannot be converted to equivalent expressions involving the total amplitude of the motion unless the polarization angle of u_{PS} is determined. Gubernatis et al. (1977, 1979) have given

general formulas for the far field scattered P and S waves and specific formulas for a few special cases of homogeneous inclusions which can be used to determine this polarization angle, but the results are not particularly simple. The second problem with these reciprocal relations is that they involve P waves and S waves incident from different directions, and the geometry of most interest in scattering problems involves P and S waves incident from the same direction.

The reciprocal relationships (D.10) and (D.11) can be further simplified in the case of symmetrical scatterers. In the case where the scattering object possesses cylindrical symmetry about the (θ_1, ϕ_1) direction, the polarization angle of u_{PS} is given by

$$\sin(\alpha_2) = \frac{\sin(\theta_1)\sin(\phi_2 - \phi_1)}{\sin(\delta)}$$

where

$$\cos(\delta) = \cos(\theta_2)\cos(\theta_1) + \sin(\theta_2)\sin(\theta_1)\cos(\phi_2 - \phi_1)$$

For an object with spherical symmetry this result holds for all directions and, furthermore, the two positions (θ_1, ϕ_1) and (θ_2, ϕ_1) can be freely interchanged. To duplicate the problem considered in this paper, let the P wave be incident from $(\theta_1 = \pi, \phi_1 = 0)$ and then

$$u_{PS}(r, \theta, \phi) = u_{PS1}(r, \theta, \phi) \hat{\theta} = -u_{PS}(r, \theta, \phi) \hat{\theta}$$

Also let the S wave be incident from this same direction $(\theta_2 = \pi, \phi_2 = 0)$ and without loss of generality take $f_{S2} = 0$. Then use (D.6) and the spherical symmetry to write

$$\begin{aligned} u_{SP}(r, \theta, \phi) &= u_{PS1}(r, \pi, 0) \\ &= \cos(\phi) u_{PS}(r, \pi, 0) \\ &= \cos(\phi) u_{S1P}(r, \theta, \phi) \end{aligned}$$

Substituting these results into (D.10) yields

$$\frac{u_{SP}(r, \theta, \phi)}{u_S^{(i)}} = -\frac{V_S^2}{V_P^2} \cos(\phi) \frac{u_{PS}(r, \theta, \phi)}{u_P^{(i)}} \quad (D.12)$$

This result is more applicable to the scattering problem as it involves the total amplitude of the P and S waves and both the incident P wave and the incident S wave arrive along the same direction. It is identical to (7.8) which was obtained from the exact far field solution for a homogeneous spherical scatterer. Note that the angle ϕ in this result is just the angle between the polarization vector of the P wave and the plane containing the polarization vector of the S wave and the scatterer.

Acknowledgements

This research was supported by Phillips Laboratory under Contract F19628-90-K-0055 and also by the U.S. Department of Energy under Contract DE-Ac03-76SF00098.

References

- Aki, K., 1969. Analysis of the seismic coda of local earthquakes as scattered waves, *J. Geophys. Res.*, **74**, 615-631.
- Aki, K., 1973. Scattering of P waves under the Montana LASA, *J. Geophys. Res.*, **79**, 1334-1346.
- Aki, K., 1980. Scattering and attenuation of shear waves in the lithosphere, *J. Geophys. Res.*, **85**, 6469-6504.
- Aki, K. (1992). Scattering conversions P to S versus S to P, *Bull. Seism. Soc. Am.*, **82**, 1969-1972.
- Gubernatis, J. E., Domany, E., and Krumhansl, J. A., 1977a. Formal aspects of the theory of the scattering of ultrasound by flaws in elastic materials, *J. Appl. Phys.*, **48**, 2804-2811.
- Gubernatis, J. E., Domany, E., Krumhansl, J. A., and Huberman, M., 1977b. The Born approximation in the theory of the scattering of elastic waves by flaws, *J. Appl. Phys.*, **48**, 2812-2819.
- Gubernatis, J. E., Krumhansl, J. A., and Thomson, R. M., 1979. Interpretation of elastic-wave scattering theory for analysis and design of flaw-characterization experiments: The long-wavelength limit, *J. Appl. Phys.*, **50**, 3338-3345.
- Haddon, R. A., and Cleary, J. R., 1974. Evidence for scattering of seismic PKP waves near the mantle-core boundary, *Phys. Earth and Planet. Int.*, **8**, 211-234.
- Korneev, V. A., 1983. About the calculation of eigenfrequencies of a radially-inhomogeneous elastic sphere, *Problems of dynamic theory of seismic wave propagation*, **23**, 26-44, Nauka, Leningrad.
- Korneev, V. A., and Petrashen, G. I., 1987. Calculation of diffraction wave fields formed on an elastic sphere, *Problems of dynamic theory of seismic wave propagation*, **27**, 26-44, Nauka, Leningrad.
- Korneev, V. A. and Johnson, L. R., 1993a. Scattering of elastic waves by a spherical inclusion - 1. Theory and numerical results, *Geophys. J. Int.*, in press.
- Korneev, V. A. and Johnson, L. R., 1993b. Scattering of elastic waves by a spherical inclusion - 2. Limitations of asymptotic solutions, *Geophys. J. Int.*, in press.
- Mie G., 1908, *Ann. de Physik* (4),25,377

- Morochnik, V. S., 1983. Scattering of shear elastic waves by a low-contrast spherical inclusion, *Izvestia Acad. Nauk USSR, Fizika Zemli*, 6, 41-49.
- Morochnik, V. S., 1983. Scattering of compressional elastic waves by a low-contrast spherical inclusion, *Izvestia Acad. Nauk USSR, Fizika Zemli*, 7, 65-72.
- Nigul, U. K. et al., 1974. *Echo-signals from elastic objects. Part 2*, Academy of Science of Estonian SSR, Tallinn, 345 pp.
- Petrashen, G.I., 1945. Solution of vector boundary problems of mathematical physics in the case of a sphere, *Doklady Acad. Nauk USSR*, 46, No. 7.
- Petrashen, G.I., 1946. Formation of oscillations and the phenomena of resonance in the case of a sphere, *Doklady Acad. Nauk USSR*, 51, No. 1.
- Petrashen, G.I., 1949. Symmetry of rotation and spherical vectors, *Scientific Papers of Leningrad State University, Series in Mathematical Sciences*, 114, 3-27.
- Petrashen, G. I., 1950a. Dynamic problem of the theory of elasticity in the case of an isotropic sphere, *Scientific Papers of Leningrad State University, Series in Mathematical Sciences*, 135, 24-70.
- Petrashen, G. I., 1950b. Oscillations of an isotropic elastic sphere. *Doklady Acad. Nauk USSR*, 47, No. 3.
- Petrashen, G. I., 1953. Methods of investigation of wave propagation in media with spherical and cylindrical boundaries, *Scientific Papers of Leningrad State University, Series in Mathematical Sciences*, 170, 27.
- Truell, R., Elbaum, C., and Chick, B. B., 1969. *Ultrasonic Methods in Solid State Physics*, Academic Press, New York.
- Van der Hulst, H. C., 1957. *Light Scattering by Small Particles*, Wiley, New York, 470 pp.
- Waterman, P. C., 1976. Matrix theory of elastic wave scattering, *J. Acoust. Soc. Am.*, 60, 567-580.
- Wu, R., and K. Aki (1985a). Scattering characteristics of elastic waves by an elastic heterogeneity, *Geophysics*, 50, 582-595.
- Wu, R., and K. Aki (1985b). Elastic wave scattering by a random medium and the small-scale inhomogeneities in the lithosphere, *J. Geophys. Res.*, 90, 10,261-10,273.
- Yamakawa, N., 1962, Scattering and attenuation of elastic waves. - *Geophys. Mag.* 31, 63-103.
- Ying, C. F. and Truell, R., 1956. Scattering of a plane longitudinal wave by a spherical obstacle in an isotropically elastic solid, *J. Appl. Phys.*, 27, 1086-1097.

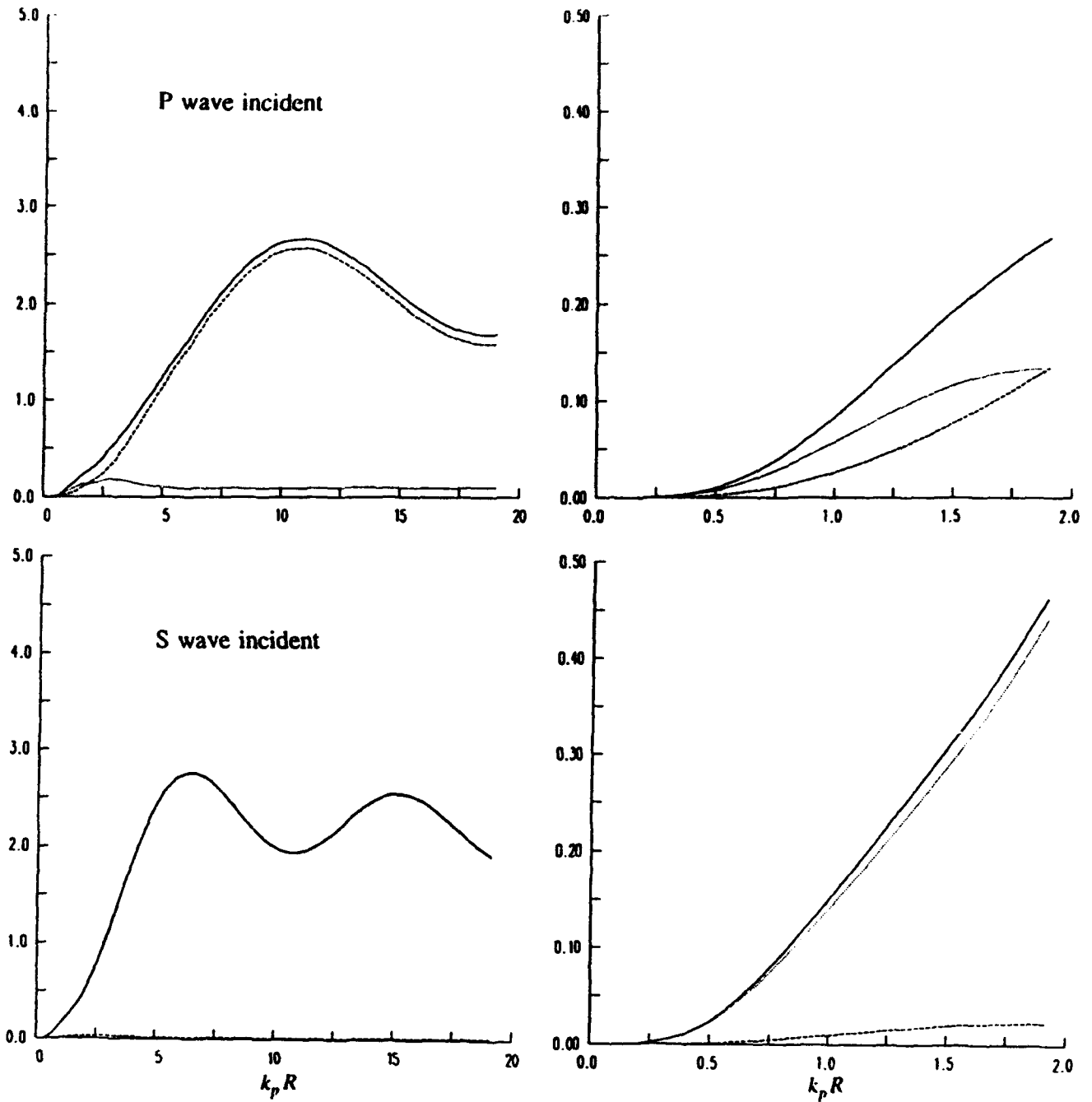


Figure 1 Normalized scattering cross sections for an elastic homogeneous sphere as a function of the parameter $k_p R = \omega R / V_p$. These results are for the high-velocity inclusion which is listed as model 1 in the text. The top two panels are for the case of an incident P wave, while the bottom two panels are for an incident S wave. The panels on the right are expanded versions of those on the left for small values of the argument. The dashed line represents the energy scattered as P waves, the dotted line represents the energy scattered as S waves, and the solid line represents the total scattered energy.

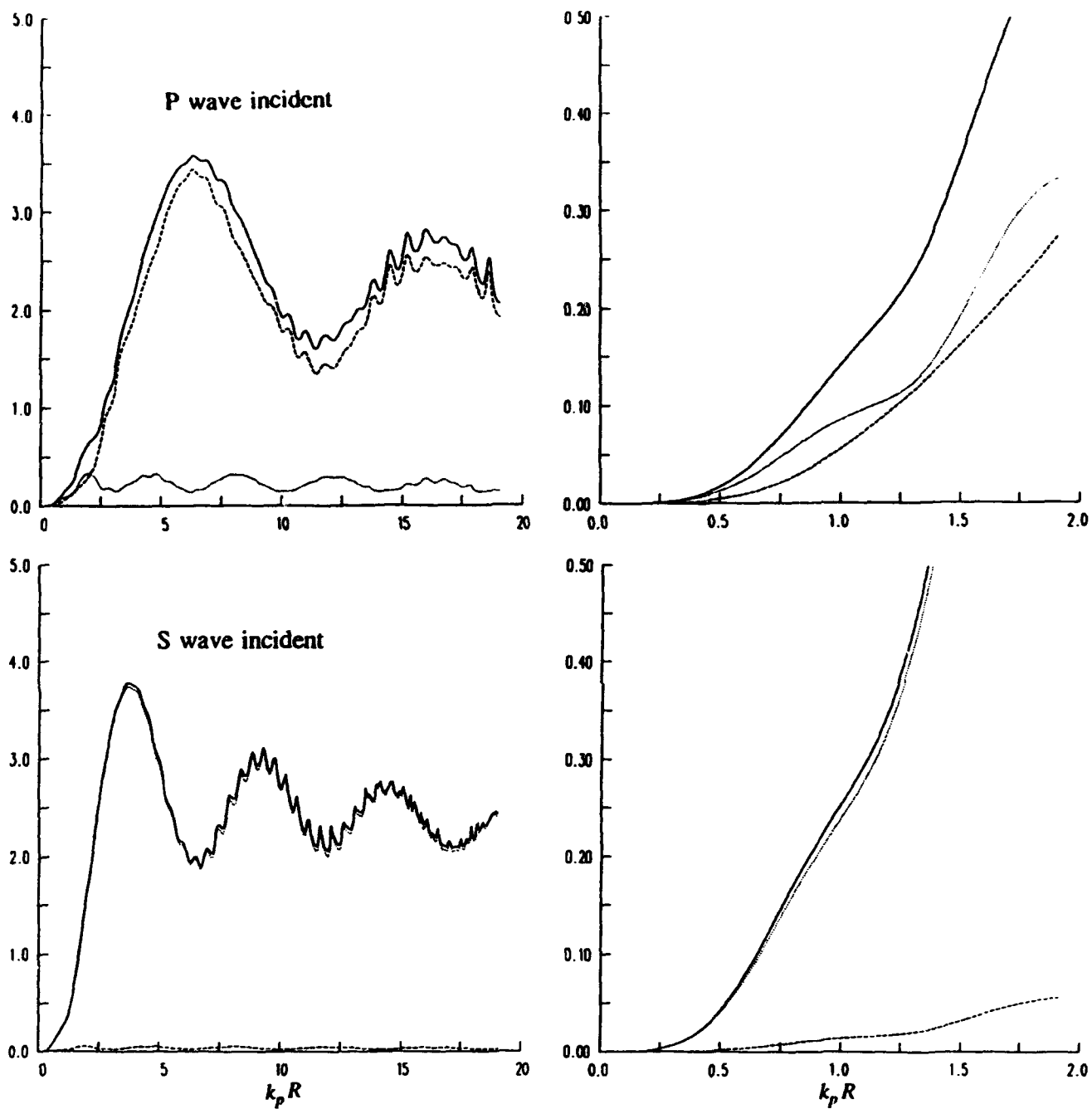


Figure 2 Similar to Figure 1 for the low-velocity inclusion which is listed as model 2 in the text.

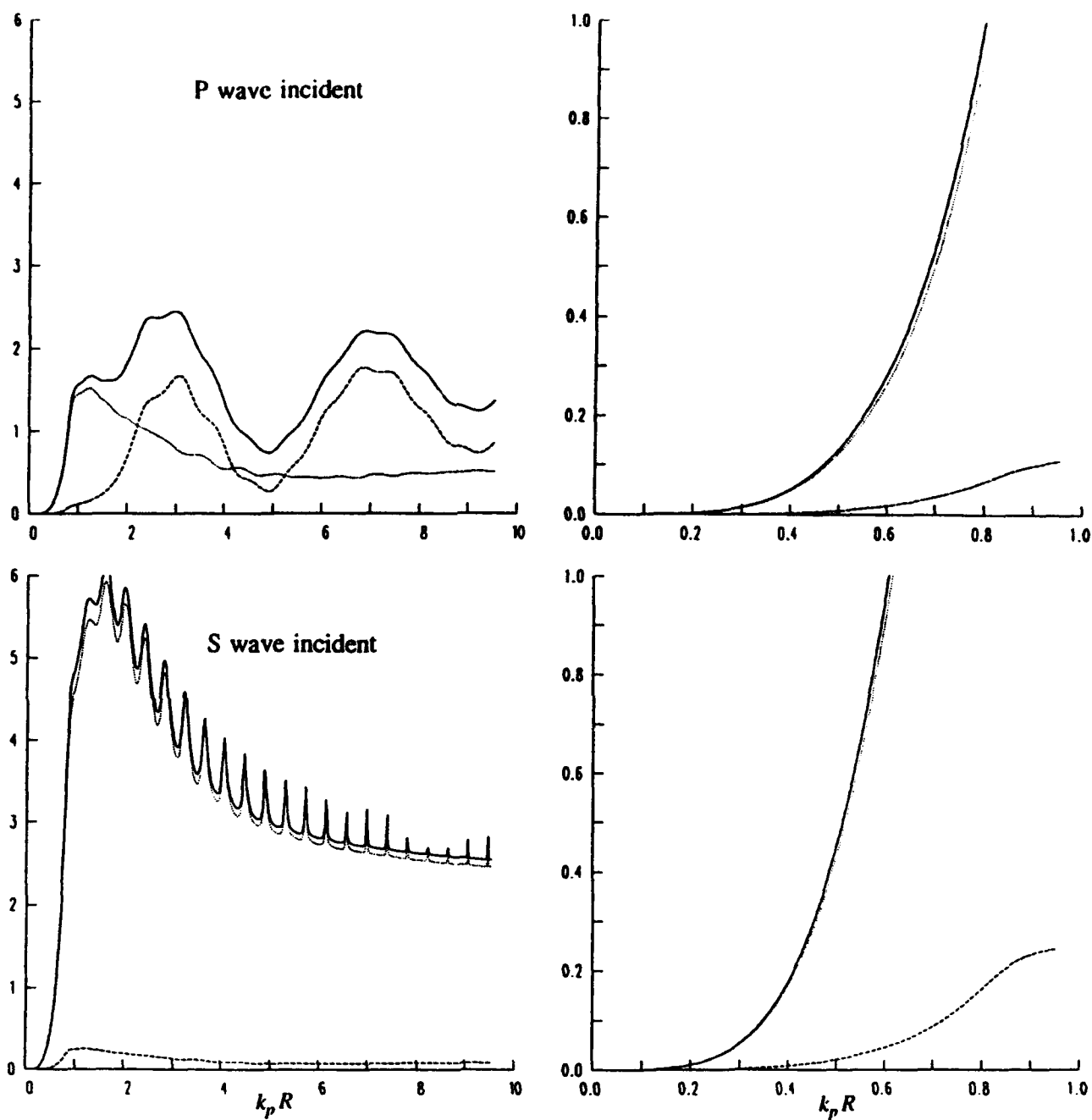


Figure 3 Similar to Figure 1 for the fluid inclusion which is listed as model 3 in the text.

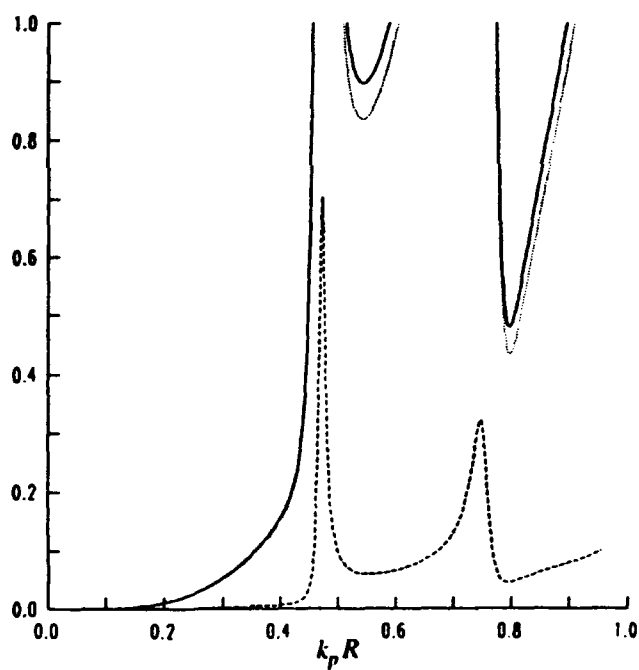
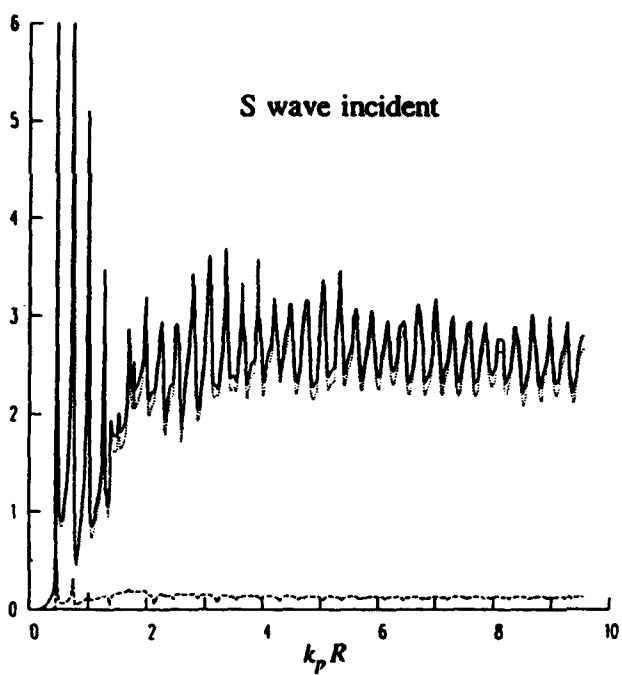
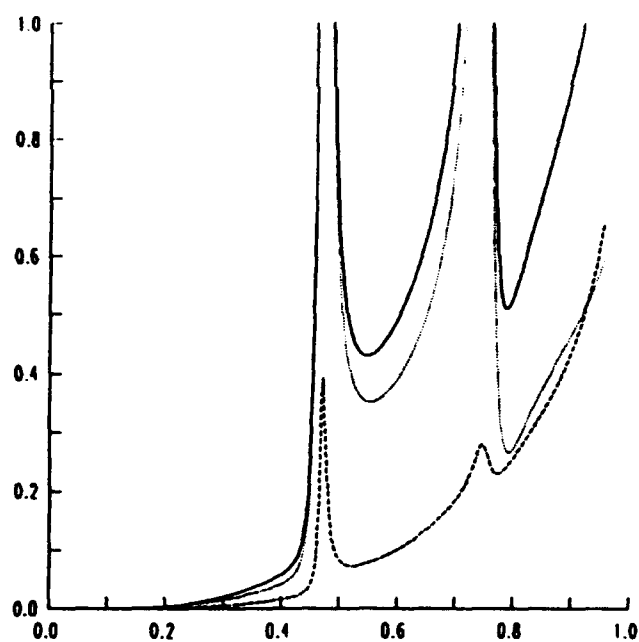
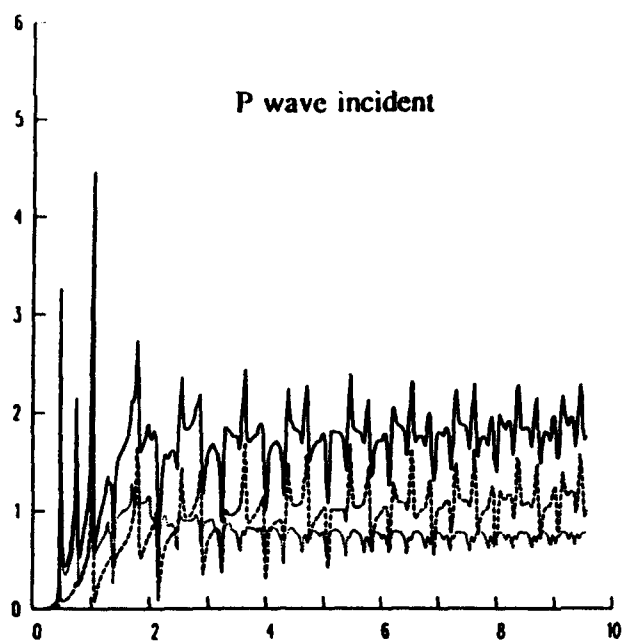


Figure 4 Similar to Figure 1 for the fluid inclusion which is listed as model 4 in the text.

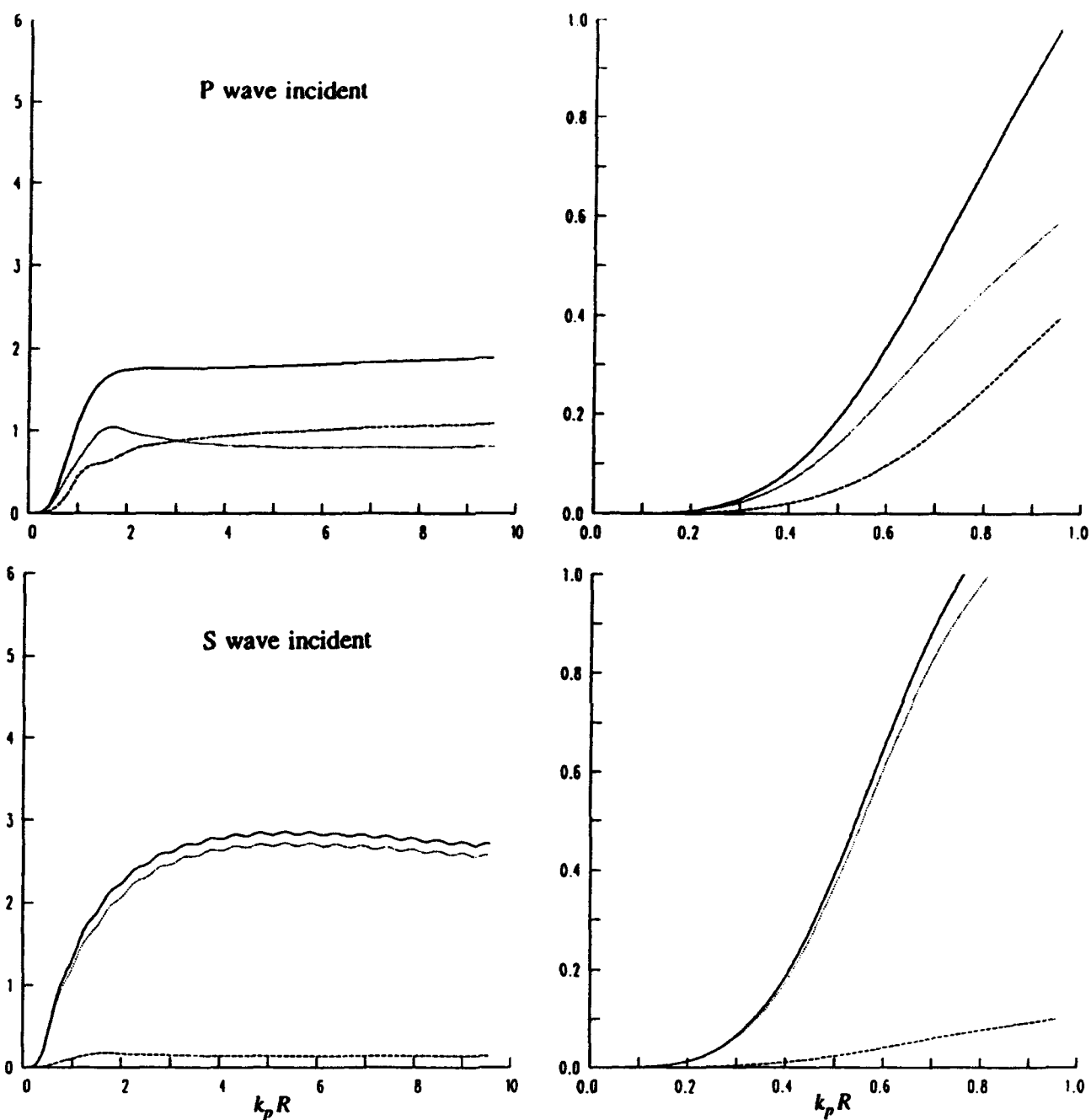


Figure 5 Similar to Figure 1 for the cavity inclusion which is listed as model 5 in the text.

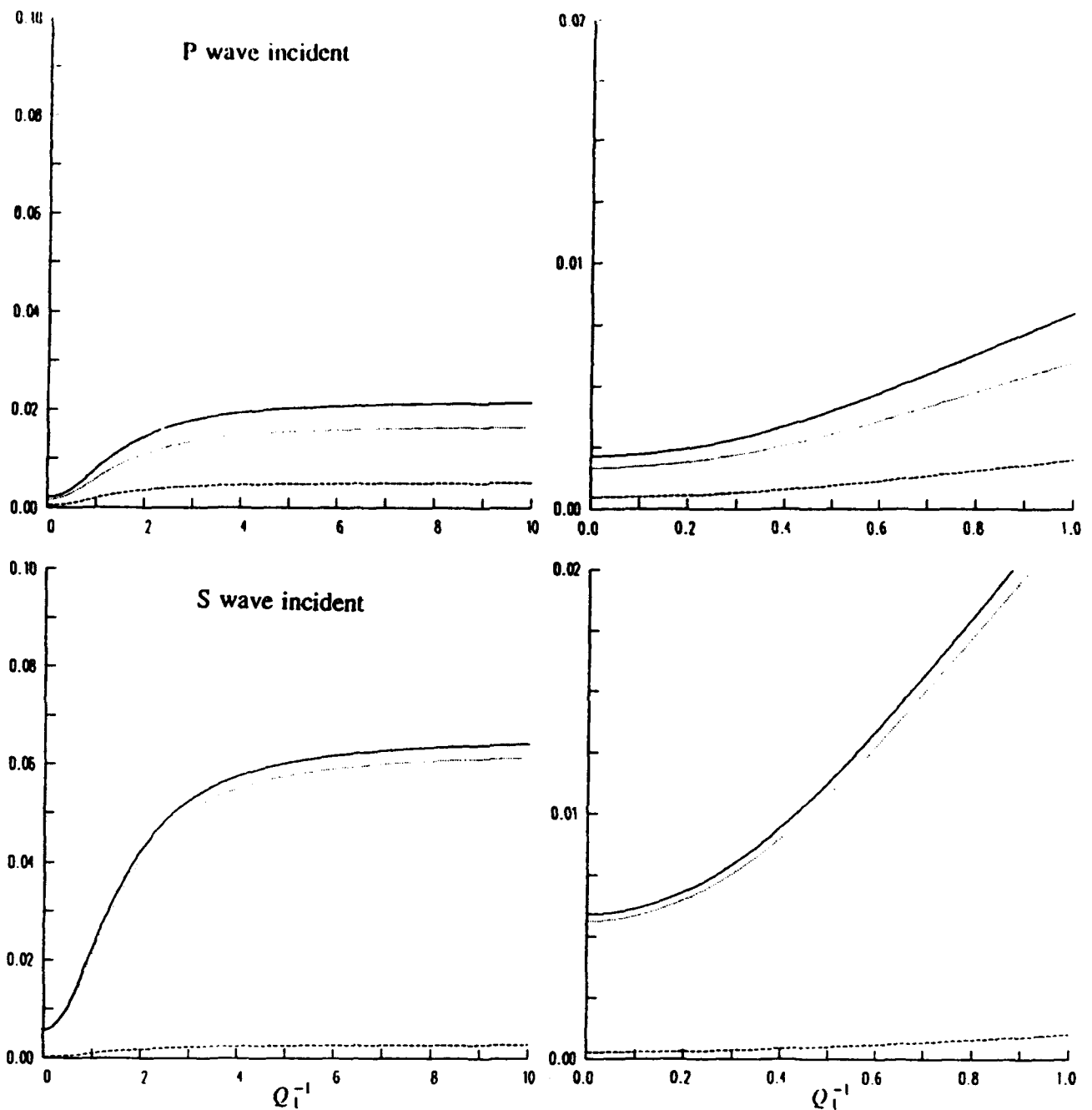


Figure 6 Normalized scattering cross sections for an anelastic homogeneous sphere as a function of the attenuation quality factor Q^{-1} of the sphere. These results are for the high-velocity inclusion which is listed as model 1 in the text with the elastic constants within the sphere modified to have complex values. The frequency is constant with $k_p R = \omega R / V_p = 0.05$. The top two panels are for the case of an incident P wave, while the bottom two panels are for an incident S wave. The panels on the right are expanded versions of those on the left for small values of the argument. The dashed line represents the energy scattered as P waves, the dotted line represents the energy scattered as S waves, and the solid line represents the total scattered energy.

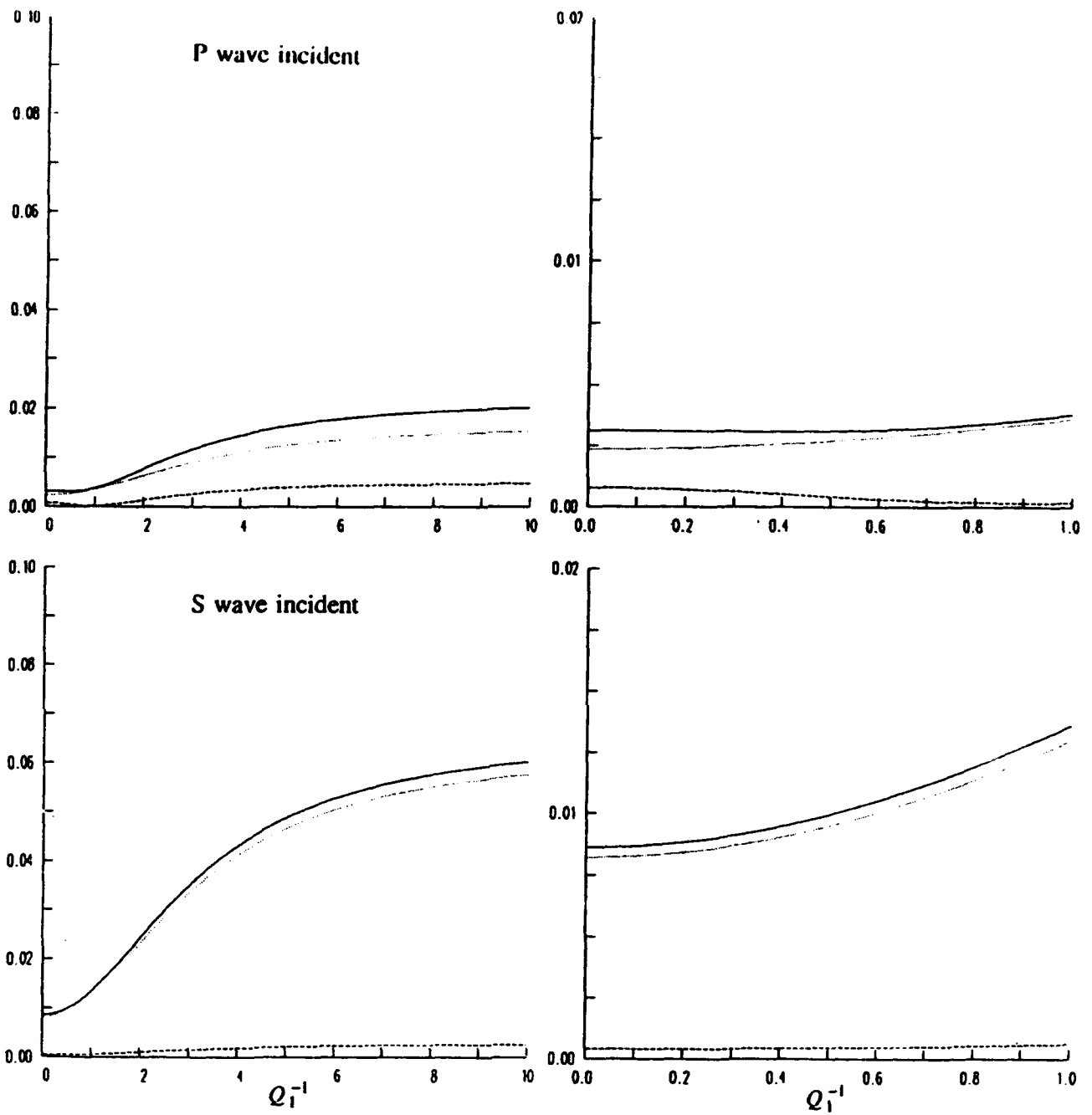


Figure 7 Similar to Figure 6 for the low-velocity inclusion which is listed as model 2 in the text.

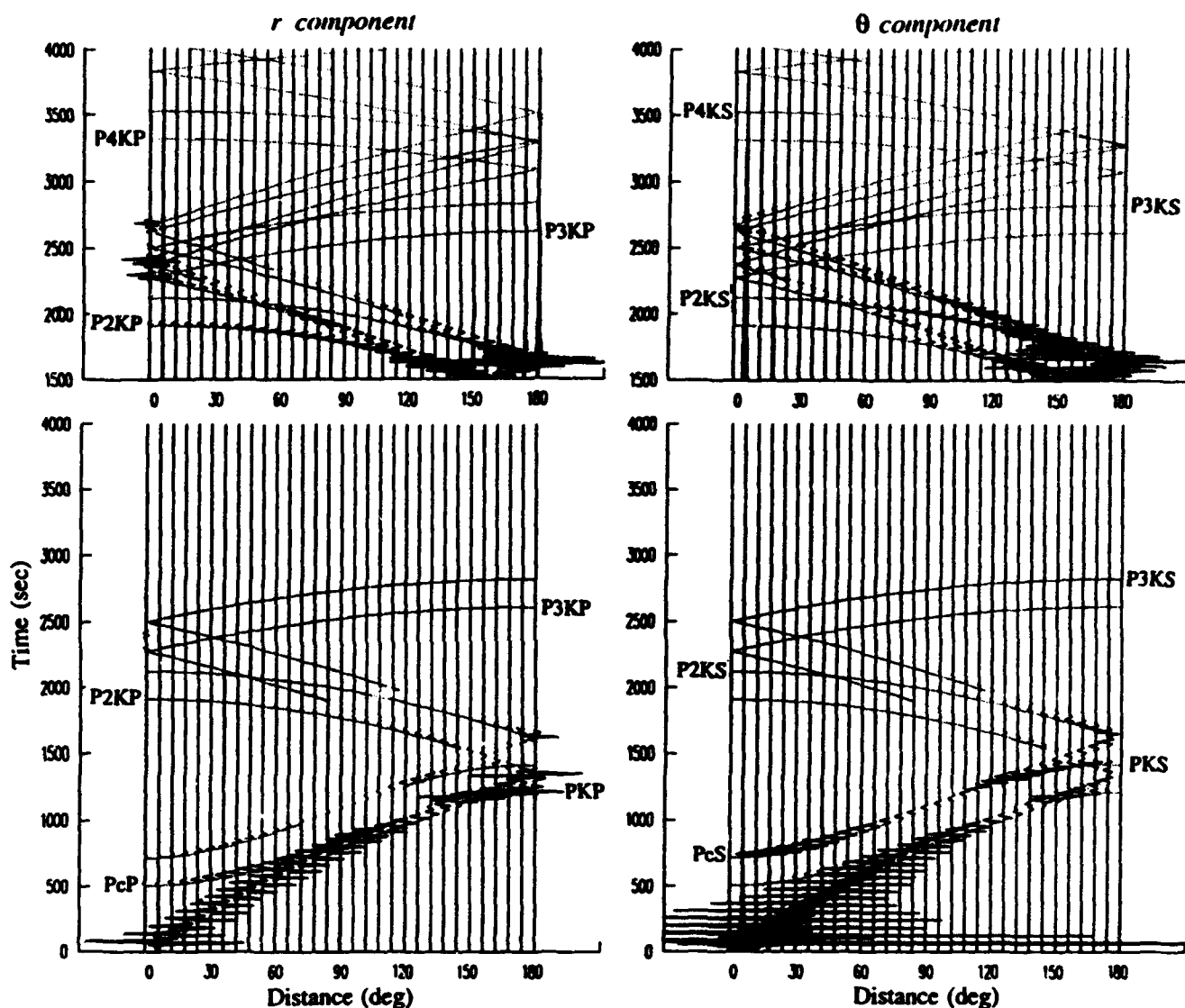


Figure 8 Synthetic seismograms calculated for a homogeneous fluid inclusion that simulates the earth's core. The seismograms are calculated every 6 degrees at a radius of 6371 km. The source is a point pressure pulse at 0 distance and a radius of 6300 km. The panels on the left are the radial components of motion and those on the right are the angular components of motion. The upper two panels are late-time versions of those below with the amplitudes increased by a factor of 10. The dotted lines are the arrival times predicted by geometrical ray theory.

Prof. Thomas Ahrens
Seismological Lab, 252-21
Division of Geological & Planetary Sciences
California Institute of Technology
Pasadena, CA 91125

Prof. Keiiti Aki
Center for Earth Sciences
University of Southern California
University Park
Los Angeles, CA 90089-0741

Prof. Shelton Alexander
Geosciences Department
403 Deike Building
The Pennsylvania State University
University Park, PA 16802

Prof. Charles B. Archambeau
CIRES
University of Colorado
Boulder, CO 80309

Dr. Thomas C. Bache, Jr.
Science Applications Int'l Corp.
10260 Campus Point Drive
San Diego, CA 92121 (2 copies)

Prof. Muawia Barazangi
Institute for the Study of the Continent
Cornell University
Ithaca, NY 14853

Dr. Jeff Barker
Department of Geological Sciences
State University of New York
at Binghamton
Vestal, NY 13901

Dr. Douglas R. Baumgardt
ENSCO, Inc
5400 Port Royal Road
Springfield, VA 22151-2388

Dr. Susan Beck
Department of Geosciences
Building #77
University of Arizona
Tucson, AZ 85721

Dr. T.J. Bennett
S-CUBED
A Division of Maxwell Laboratories
11800 Sunrise Valley Drive, Suite 1212
Reston, VA 22091

Dr. Robert Blandford
AFTAC/TT, Center for Seismic Studies
1300 North 17th Street
Suite 1450
Arlington, VA 22209-2308

Dr. Stephen Bratt
ARPA/NMRO
3701 North Fairfax Drive
Arlington, VA 22203-1714

Dr. Lawrence Burdick
IGPP, A-025
Scripps Institute of Oceanography
University of California, San Diego
La Jolla, CA 92093

Dr. Robert Burrige
Schlumberger-Doll Research Center
Old Quarry Road
Ridgefield, CT 06877

Dr. Jerry Carter
Center for Seismic Studies
1300 North 17th Street
Suite 1450
Arlington, VA 22209-2308

Dr. Eric Chael
Division 9241
Sandia Laboratory
Albuquerque, NM 87185

Dr. Martin Chapman
Department of Geological Sciences
Virginia Polytechnical Institute
21044 Derring Hall
Blacksburg, VA 24061

Prof. Vernon F. Cormier
Department of Geology & Geophysics
U-45, Room 207
University of Connecticut
Storrs, CT 06268

Prof. Steven Day
Department of Geological Sciences
San Diego State University
San Diego, CA 92182

Marvin Denny
U.S. Department of Energy
Office of Arms Control
Washington, DC 20585

Dr. Zoltan Der
ENSCO, Inc.
5400 Port Royal Road
Springfield, VA 22151-2388

Dr. Cliff Frolich
Institute of Geophysics
8701 North Mopac
Austin, TX 78759

Prof. Adam Dziewonski
Hoffman Laboratory, Harvard University
Dept. of Earth Atmos. & Planetary Sciences
20 Oxford Street
Cambridge, MA 02138

Dr. Holly Given
IGPP, A-025
Scripps Institute of Oceanography
University of California, San Diego
La Jolla, CA 92093

Prof. John Ebel
Department of Geology & Geophysics
Boston College
Chestnut Hill, MA 02167

Dr. Jeffrey W. Given
SAIC
10260 Campus Point Drive
San Diego, CA 92121

Eric Fielding
SNEE Hall
INSTOC
Cornell University
Ithaca, NY 14853

Dr. Dale Glover
Defense Intelligence Agency
ATTN: ODT-1B
Washington, DC 20301

Dr. Petr Firbas
Institute of Physics of the Earth
Masaryk University Brno
Jecna 29a
612 46 Brno, Czech Republic

Dan N. Hagedorn
Pacific Northwest Laboratories
Battelle Boulevard
Richland, WA 99352

Dr. Mark D. Fisk
Mission Research Corporation
735 State Street
P.O. Drawer 719
Santa Barbara, CA 93102

Dr. James Hannon
Lawrence Livermore National Laboratory
P.O. Box 808
L-205
Livermore, CA 94550

Prof Stanley Flatte
Applied Sciences Building
University of California, Santa Cruz
Santa Cruz, CA 95064

Prof. David G. Harkrider
Seismological Laboratory
Division of Geological & Planetary Sciences
California Institute of Technology
Pasadena, CA 91125

Dr. John Foley
NER-Geo Sciences
1100 Crown Colony Drive
Quincy, MA 02169

Prof. Danny Harvey
CIRES
University of Colorado
Boulder, CO 80309

Prof. Donald Forsyth
Department of Geological Sciences
Brown University
Providence, RI 02912

Prof. Donald V. Helmberger
Seismological Laboratory
Division of Geological & Planetary Sciences
California Institute of Technology
Pasadena, CA 91125

Dr. Art Frankel
U.S. Geological Survey
922 National Center
Reston, VA 22092

Prof. Eugene Herrin
Institute for the Study of Earth and Man
Geophysical Laboratory
Southern Methodist University
Dallas, TX 75275

Prof. Robert B. Herrmann
Department of Earth & Atmospheric Sciences
St. Louis University
St. Louis, MO 63156

Prof. Lane R. Johnson
Seismographic Station
University of California
Berkeley, CA 94720

Prof. Thomas H. Jordan
Department of Earth, Atmospheric &
Planetary Sciences
Massachusetts Institute of Technology
Cambridge, MA 02139

Prof. Alan Kafka
Department of Geology & Geophysics
Boston College
Chestnut Hill, MA 02167

Robert C. Kemerait
ENSCO, Inc.
445 Pineda Court
Melbourne, FL 32940

Dr. Karl Koch
Institute for the Study of Earth and Man
Geophysical Laboratory
Southern Methodist University
Dallas, Tx 75275

Dr. Max Koontz
U.S. Dept. of Energy/DP 5
Forrestal Building
1000 Independence Avenue
Washington, DC 20585

Dr. Richard LaCoss
MIT Lincoln Laboratory, M-200B
P.O. Box 73
Lexington, MA 02173-0073

Dr. Fred K. Lamb
University of Illinois at Urbana-Champaign
Department of Physics
1110 West Green Street
Urbana, IL 61801

Prof. Charles A. Langston
Geosciences Department
403 Deike Building
The Pennsylvania State University
University Park, PA 16802

Jim Lawson, Chief Geophysicist
Oklahoma Geological Survey
Oklahoma Geophysical Observatory
P.O. Box 8
Leonard, OK 74043-0008

Prof. Thorne Lay
Institute of Tectonics
Earth Science Board
University of California, Santa Cruz
Santa Cruz, CA 95064

Dr. William Leith
U.S. Geological Survey
Mail Stop 928
Reston, VA 22092

Mr. James F. Lewkowicz
Phillips Laboratory/GPEH
29 Randolph Road
Hanscom AFB, MA 01731-3010(2 copies)

Mr. Alfred Lieberman
ACDA/VI-OA State Department Building
Room 5726
320-21st Street, NW
Washington, DC 20451

Prof. L. Timothy Long
School of Geophysical Sciences
Georgia Institute of Technology
Atlanta, GA 30332

Dr. Randolph Martin, III
New England Research, Inc.
76 Olcott Drive
White River Junction, VT 05001

Dr. Robert Masse
Denver Federal Building
Box 25046, Mail Stop 967
Denver, CO 80225

Dr. Gary McCartor
Department of Physics
Southern Methodist University
Dallas, TX 75275

Prof. Thomas V. McEvelly
Seismographic Station
University of California
Berkeley, CA 94720

Dr. Art McGarr
U.S. Geological Survey
Mail Stop 977
U.S. Geological Survey
Menlo Park, CA 94025

Dr. Keith L. McLaughlin
S-CUBED
A Division of Maxwell Laboratory
P.O. Box 1620
La Jolla, CA 92038-1620

Stephen Miller & Dr. Alexander Florence
SRI International
333 Ravenswood Avenue
Box AF 116
Menlo Park, CA 94025-3493

Prof. Bernard Minster
IGPP, A-025
Scripps Institute of Oceanography
University of California, San Diego
La Jolla, CA 92093

Prof. Brian J. Mitchell
Department of Earth & Atmospheric Sciences
St. Louis University
St. Louis, MO 63156

Mr. Jack Murphy
S-CUBED
A Division of Maxwell Laboratory
11800 Sunrise Valley Drive, Suite 1212
Reston, VA 22091 (2 Copies)

Dr. Keith K. Nakanishi
Lawrence Livermore National Laboratory
L-025
P.O. Box 808
Livermore, CA 94550

Prof. John A. Orcutt
IGPP, A-025
Scripps Institute of Oceanography
University of California, San Diego
La Jolla, CA 92093

Prof. Jeffrey Park
Kline Geology Laboratory
P.O. Box 6666
New Haven, CT 06511-8130

Dr. Howard Patton
Lawrence Livermore National Laboratory
L-025
P.O. Box 808
Livermore, CA 94550

Dr. Frank Pilotte
HQ AFTAC/TT
1030 South Highway A1A
Patrick AFB, FL 32925-3002

Dr. Jay J. Pulli
Radix Systems, Inc.
201 Perry Parkway
Gaithersburg, MD 20877

Dr. Robert Reinke
ATTN: FCTVTD
Field Command
Defense Nuclear Agency
Kirtland AFB, NM 87115

Prof. Paul G. Richards
Lamont-Doherty Geological Observatory
of Columbia University
Palisades, NY 10964

Mr. Wilmer Rivers
Teledyne Geotech
314 Montgomery Street
Alexandria, VA 22314

Dr. Alan S. Ryall, Jr.
ARPA/NMRO
3701 North Fairfax Drive
Arlington, VA 22203-1714

Dr. Richard Sailor
TASC, Inc.
55 Walkers Brook Drive
Reading, MA 01867

Prof. Charles G. Sammis
Center for Earth Sciences
University of Southern California
University Park
Los Angeles, CA 90089-0741

Prof. Christopher H. Scholz
Lamont-Doherty Geological Observatory
of Columbia University
Palisades, NY 10964

Dr. Susan Schwartz
Institute of Tectonics
1156 High Street
Santa Cruz, CA 95064

Secretary of the Air Force
(SAFRD)
Washington, DC 20330

Office of the Secretary of Defense
DDR&E
Washington, DC 20330

Thomas J. Sereno, Jr.
Science Application Int'l Corp.
10260 Campus Point Drive
San Diego, CA 92121

Dr. Michael Shore
Defense Nuclear Agency/SPSS
6801 Telegraph Road
Alexandria, VA 22310

Dr. Robert Shumway
University of California Davis
Division of Statistics
Davis, CA 95616

Dr. Matthew Sibol
Virginia Tech
Seismological Observatory
4044 Derring Hall
Blacksburg, VA 24061-0420

Prof. David G. Simpson
IRIS, Inc.
1616 North Fort Myer Drive
Suite 1050
Arlington, VA 22209

Donald L. Springer
Lawrence Livermore National Laboratory
L-025
P.O. Box 808
Livermore, CA 94550

Dr. Jeffrey Stevens
S-CUBED
A Division of Maxwell Laboratory
P.O. Box 1620
La Jolla, CA 92038-1620

Lt. Col. Jim Stobie
ATTN: AFOSR/NL
110 Duncan Avenue
Bolling AFB
Washington, DC 20332-0001

Prof. Brian Stump
Institute for the Study of Earth & Man
Geophysical Laboratory
Southern Methodist University
Dallas, TX 75275

Prof. Jeremiah Sullivan
University of Illinois at Urbana-Champaign
Department of Physics
1110 West Green Street
Urbana, IL 61801

Prof. L. Sykes
Lamont-Doherty Geological Observatory
of Columbia University
Palisades, NY 10964

Dr. David Taylor
ENSCO, Inc.
445 Pineda Court
Melbourne, FL 32940

Dr. Steven R. Taylor
Los Alamos National Laboratory
P.O. Box 1663
Mail Stop C335
Los Alamos, NM 87545

Prof. Clifford Thurber
University of Wisconsin-Madison
Department of Geology & Geophysics
1215 West Dayton Street
Madison, WS 53706

Prof. M. Nafi Toksoz
Earth Resources Lab
Massachusetts Institute of Technology
42 Carleton Street
Cambridge, MA 02142

Dr. Larry Turnbull
CIA-OSWR/NED
Washington, DC 20505

Dr. Gregory van der Vink
IRIS, Inc.
1616 North Fort Myer Drive
Suite 1050
Arlington, VA 22209

Dr. Karl Veith
EG&G
5211 Auth Road
Suite 240
Suitland, MD 20746

Prof. Terry C. Wallace
Department of Geosciences
Building #77
University of Arizona
Tuscon, AZ 85721

Phillips Laboratory
ATTN: GPE
29 Randolph Road
Hanscom AFB, MA 01731-3010

Dr. Thomas Weaver
Los Alamos National Laboratory
P.O. Box 1663
Mail Stop C335
Los Alamos, NM 87545

Phillips Laboratory
ATTN: TSML
5 Wright Street
Hanscom AFB, MA 01731-3004

Dr. William Wortman
Mission Research Corporation
8560 Cinderbed Road
Suite 700
Newington, VA 22122

Phillips Laboratory
ATTN: PL/SUL
3550 Aberdeen Ave SE
Kirtland, NM 87117-5776 (2 copies)

Prof. Francis T. Wu
Department of Geological Sciences
State University of New York
at Binghamton
Vestal, NY 13901

Dr. Michel Bouchon
I.R.I.G.M.-B.P. 68
38402 St. Martin D'Herès
Cedex, FRANCE

ARPA, OASB/Library
3701 North Fairfax Drive
Arlington, VA 22203-1714

Dr. Michel Campillo
Observatoire de Grenoble
I.R.I.G.M.-B.P. 53
38041 Grenoble, FRANCE

HQ DNA
ATTN: Technical Library
Washington, DC 20305

Dr. Kin Yip Chun
Geophysics Division
Physics Department
University of Toronto
Ontario, CANADA

Defense Intelligence Agency
Directorate for Scientific & Technical Intelligence
ATTN: DTIB
Washington, DC 20340-6158

Prof. Hans-Peter Harjes
Institute for Geophysics
Ruhr University/Bochum
P.O. Box 102148
4630 Bochum 1, GERMANY

Defense Technical Information Center
Cameron Station
Alexandria, VA 22314 (2 Copies)

Prof. Eystein Husebye
NTNF/NORSAR
P.O. Box 51
N-2007 Kjeller, NORWAY

TACTEC
Battelle Memorial Institute
505 King Avenue
Columbus, OH 43201 (Final Report)

David Jepsen
Acting Head, Nuclear Monitoring Section
Bureau of Mineral Resources
Geology and Geophysics
G.P.O. Box 378, Canberra, AUSTRALIA

Phillips Laboratory
ATTN: XPG
29 Randolph Road
Hanscom AFB, MA 01731-3010

Ms. Eva Johannisson
Senior Research Officer
FOA
S-172 90 Sundbyberg, SWEDEN

Dr. Peter Marshall
Procurement Executive
Ministry of Defense
Blacknest, Brimpton
Reading FG7-FRS, UNITED KINGDOM

• Dr. Bernard Massinon, Dr. Pierre Mechler
Societe Radiomana
27 rue Claude Bernard
• 75005 Paris, FRANCE (2 Copies)

Dr. Svein Mykkeltveit
NTNT/NORSAR
P.O. Box 51
N-2007 Kjeller, NORWAY (3 Copies)

Prof. Keith Priestley
University of Cambridge
Bullard Labs, Dept. of Earth Sciences
Madingley Rise, Madingley Road
Cambridge CB3 0EZ, ENGLAND

Dr. Jorg Schlittenhardt
Federal Institute for Geosciences & Nat'l Res.
Postfach 510153
D-30631 Hannover, GERMANY

Dr. Johannes Schweitzer
Institute of Geophysics
Ruhr University/Bochum
P.O. Box 1102148
4360 Bochum 1, GERMANY

Trust & Verify
VERTIC
Carrara House
20 Embankment Place
London WC2N 6NN, ENGLAND